Robotica (2012) volume 30, pp. 257–278. © Cambridge University Press 2011
doi:10.1017/S0263574711000555

# Smooth gait optimization of a fish robot using the genetic-hill climbing algorithm

Tuong Quan Vo, Hyoung Seok Kim and *Byung Ryong Lee

*School of Mechanical and Automotive Engineering, University of Ulsan, San 29, Mugeo 2-dong, Nam-gu, Ulsan 680-749, South Korea*

(Received in Final Form: May 11, 2011; accepted May 6, 2011. First published online: June 14, 2011)

**SUMMARY**

This paper presents a model of a three-joint (four links) carangiform fish robot. The smooth gait or smooth motion of a fish robot is optimized by using a combination of the Genetic Algorithm (GA) and the Hill Climbing Algorithm (HCA) with respect to its dynamic system. Genetic algorithm is used to create an initial set of optimal parameters for the two input torque functions of the system. This set is then optimized by using HCA to ensure that the final set of optimal parameters is a "near" global optimization result. Finally, the simulation results are presented in order to demonstrate that the proposed method is effective.

KEYWORDS: Fish robot; Dynamic; Optimization, GA; HCA; Smooth gait; Input torque; Big jump.

## 1. Introduction

Many research studies about underwater propulsion depend on the use of propellers or thrusters, or buoyancy to generate the motion of objects in the underwater environment. Thruster is mostly used in Remotely Operated Vehicles (ROVs) or Autonomous Underwater Vehicles (AUVs) to create the propulsion force for the robot's movement. Sun and Cheah[1] used thruster to generate the propulsion force for their AUV. Besides, McFarland *et al.*[2] employed the buoyancy control inspired by sperm whales to operate their bio-mimetic underwater robot. However, most natural methods for underwater propulsion employ the change of an object's body shape to create movement. Changing the body shape generates propulsion force for fish robot, which makes fish robot move forward effectively.

The carangiform fish robot is an example of changing an object's body shape to move itself in an underwater environment.

Lauder and Drucker[3] performed thorough surveys and analyzed the motion mechanisms of fish fins to develop a successful underwater robot system. Lighthill[4] also studied the hydromechanics of aquatic animal propulsion because many underwater animals whose motion mechanisms have evolved over many generations adapted to the harsh conditions of the underwater environment. Other studies have investigated this type of motion, which is based on natural movement. Yu and Wang[5] calculated the optimal link ratio of a four-link fish robot by using computer simulations and compared the moving speed of two types of models. One model used in this comparison utilized the optimal link ratio and the other model was considered without the optimal link ratio. In recent years, some new technologies related to intelligent control techniques used to optimize the movement of fish robots have been developed. Zhao *et al.*[6] and Zhang *et al.*[7] used the concept of a bionic neural network, called the Central Pattern Generator (CPG) to create the motions for their fish robot. This concept is a new application of intelligent control in a fish robot controller. Besides, Liu *et al.*[8] proposed a modular approach to decompose fish movement into several basic behaviors, namely straight cruise, cruise in turn, and sharp turn, to mimic carangiform swimming of a real fish.

However, most research about fish robots is based on a simplified model of fish robot kinematics and experimental approaches. Yu *et al.*[9] made an improved approach to design a robot fish based on a simplified kinematics model that relates frequency to speed and joint angle bias to turn, where geometric reduction is employed and complex hydrodynamic analysis is avoided.

In our research, we considered a 3-joint (4-link) carangiform fish robot-type. The dynamic model of this robot was derived by using the Lagrange method. The influence of fluid force on the motion of fish robot was also considered, based on Lighthill's study of carangiform propulsion.[10] In addition, the Singular Value Decomposition (SVD) algorithm is used in our simulation program to minimize the divergence of a fish robot's links when simulating the motion of a fish robot in an underwater environment. A fish robot achieves a smooth gait or smooth motion if the displacement of its links' positions from the current sampling time ($t_i$) to the next sampling time ($t_{i+1}$) is small or the displacement positions during numerous sampling points are regular. The idea of regulation is that there is no big jump or big gap in positional displacement between two consecutive positions of the fish robot's links during the operation time. In addition, the displacement positions between two consecutive positions of the fish robot's links in numerous sampling points are quite equal or identical. We do not pay much attention to the motion of head and body of a fish robot because a real carangiform fish has very small undulation motion in the parts.

The main goal of this paper is to develop a method to determine the optimal set of parameters that make fish robot

* Corresponding Author: E-mail: brlee@ulsan.ac.kr

https://doi.org/10.1017/S0263574711000555 Published online by Cambridge University Press

generate a smooth gait or smooth motion, similar to a real fish. In our research, a fish robot should achieve forward motion in two dimensions. The movement of a fish robot in an underwater environment should be generated by its body motion and its tail fin. A fish robot can achieve a smooth gait if the optimal input torque functions are applied to its dynamic model. The optimal input torque functions are determined by optimizing the parameters that are used to build these input functions. The proposed method for achieving a smooth gait is to combine GA and HCA to solve the optimization problem of fish robot's motion with respect to its dynamic model and other related constraints. Another solution to achieve a smooth gait in a fish robot was proposed by Seo *et al.*[11] They used numerical optimization software (NLPP – Non-Linear Path Planning – Tool Box for Matlab) to optimize the control parameters for a simplified planar model of a carangiform fish robot.

This paper is organized as follows. The motion equations of a fish robot are introduced in Section 2. A brief review of GA–HCA and the application of these optimization methods to investigate the smooth gait problem in fish robots are presented in Section 3. Some simulation results are introduced in Section 4. Then some preliminary experiments are conducted in Section 5 to prove the effectiveness of the proposed method. Finally, our conclusion and some suggestions for future work are provided in Sections 6 and 7, respectively.

## 2. Motion Equations of a Fish Robot

A carangiform fish, many researchers' interest, is one of the most popular body and/or caudal fin (BCF) fish. Guo developed a control system for the waypoint-tracking of a biomimetic autonomous underwater vehicle (BAUV).[12] A BAUV swims forward by oscillating its body and caudal fin.[12] Liu and Hu build a simulation environment for optimizing control parameters of their carangiform fish robot.[13] The simulation environment is a convenient way to develop and test the motion control algorithm for a robotic fish.[13] In a quite similar research about simulation method, Borazjani and Sotiropoulos[14] introduced a numerical investigation of hydrodynamics of carangiform swimming in the transitional and flow regimes. They employed numerical simulation to investigate the hydrodynamics of carangiform locomotion as the relative magnitude of viscous and inertial forces, where Reynolds number (Re), tail-beat frequency, and Strouhal number (St) were systematically varied.[14] Another research on the motion of a fish robot in BCF and median and/or paired fin (MPF) was done by Low *et al.*[15] They discussed a mechanism design and gait study of a biomimetic fish robot in two major forms of planar serial chain mechanism and parallel mechanism. Besides, gait functions for two forms of a biomimetic fish robot were also discussed by the authors.[15]

In developing our fish robot, we mainly focus on a carangiform fish because of its fast swimming capability, which resembles that of a trout or a mackerel and, in addition, the fish has a large and high-aspect-ratio tail.[16]

The movement of this fish requires powerful muscles that generate motion side-to-side through the posterior part, while the anterior part of the body remains relatively motionless as shown in Fig. 1.

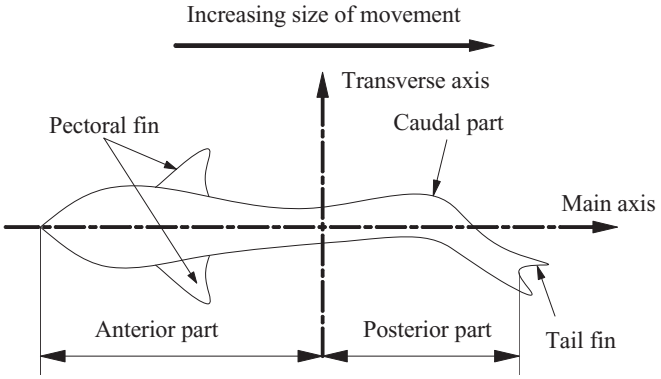



Fig. 1. Carangiform locomotion style.

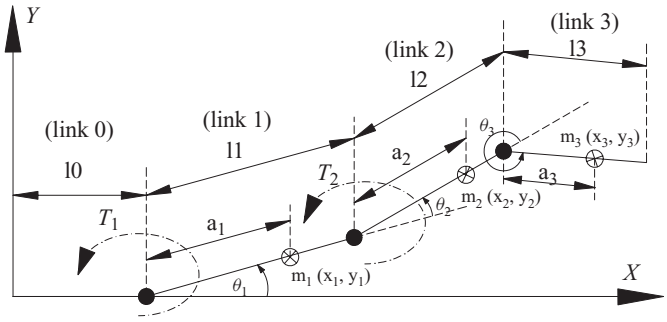



Fig. 2. Fish robot analytical model.

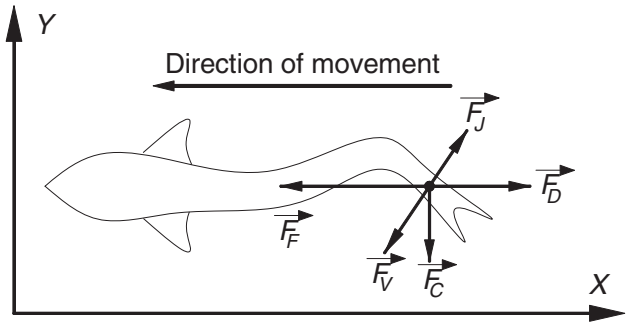



Fig. 3. Distribution of forces on fish robot.

We design a 3-joint (4-link) fish robot in order to obtain a smoother and more natural motion for the robot. The analytical model of the fish robot is introduced in Fig. 2.

In Fig. 2, $T_1$ and $T_2$ are the input torques at joint 1 and joint 2, which are generated by using two active DC motors. We assume that the inertial fluid force $F_V$ and the lift force $F_J$ act on the tail fin only (link 3), which is similar to the hypothesis developed by Nakashima *et al.*[17] The distribution of forces exerted on fish robot is presented in Fig. 3. $F_F$ is the thrust force component at the tail fin, $F_C$ is the lateral force component, and $F_D$ is the drag force, all of which affect fish robot's motion. These forces were calculated in a similar manner as that of Nakashima *et al.*'s method used with their 2-joint fish robot.[17]

We suppose that the tail fin of a fish robot is in constant flow $U_m$, so we can conclude that the inertial fluid force and the lift force act on the tail fin of a fish robot. Then we can calculate their thrust component $F_F$ and lateral component

https://doi.org/10.1017/S0263574711000555 Published online by Cambridge University Press

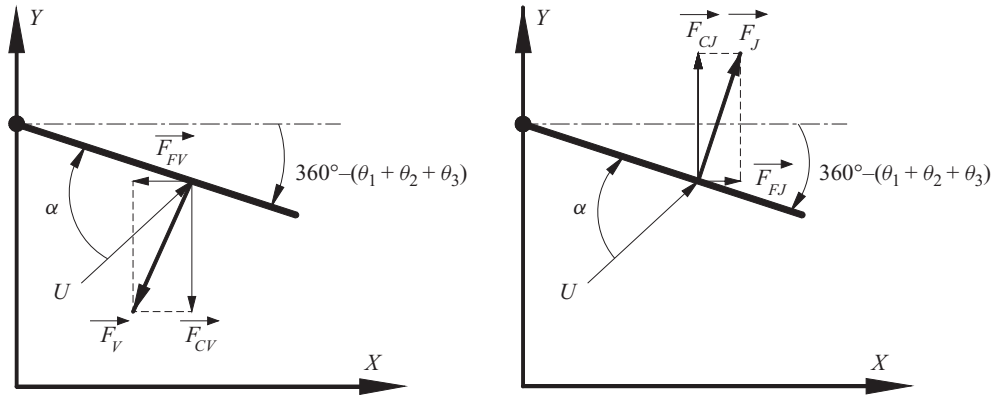



Fig. 4. Model of inertial fluid force and lift force.

$F_C$ from the inertial fluid force and lift force. As the fish robot is tested in a tank of water, the value of $U_m$ is set to be 0.08 m/s. In Fig. 4, $F_v$ is the force proportional to the acceleration acting from the opposite direction of the acceleration.[17] $F_V$ is calculated in Eq. (1).[17] The lift force $F_J$ is perpendicular to the flow, and it is calculated in Eq. (2).[17] In these two equations, the chord length is $2C$, the span of the tail fin is $L$, and $\rho$ is the density of the water.

$$F_V = \pi\rho LC^2\dot{U}\sin\alpha + \pi\rho LC^2\dot{\alpha}U\cos\alpha, \tag{1}$$

$$F_J = 2\pi\rho LCU^2\sin\alpha\cos\alpha. \tag{2}$$

The fluid force and lift force are divided into a thrust component, $F_F$, in direction $x$ and a lateral force component, $F_C$, in direction $y$ as shown in Fig. 4.

In Fig. 4, $U$ is the relative velocity at the center of the tail fin and $\alpha$ is the attack angle. As shown in Fig. 4, the values of $F_F$ and $F_C$ can be calculated as shown in Eqs. (3) and (4):

$$F_F = F_{FV} - F_{FJ} = F_V\sin(360^\circ - (\theta_1+\theta_2+\theta_3)) - F_J\sin(360^\circ - (\theta_1+\theta_2+\theta_3)), \tag{3}$$

$$F_C = F_{CV} - F_{CJ} = F_V\cos(360^\circ - (\theta_1+\theta_2+\theta_3)) - F_J\cos(360^\circ - (\theta_1+\theta_2+\theta_3)). \tag{4}$$

These two equations can be simplified as follows:

$$F_F = -F_V\sin(\theta_1+\theta_2+\theta_3) + F_J\sin(\theta_1+\theta_2+\theta_3), \tag{5}$$

$$F_C = F_V\cos(\theta_1+\theta_2+\theta_3) - F_J\cos(\theta_1+\theta_2+\theta_3). \tag{6}$$

If we consider only the movement of the fish robot in direction $x$, the relative velocity in direction $y$ at the center of tail fin is calculated by Eq. (7),

$$u = \dot{\theta}_1 l_1\cos\theta_1 + (\dot{\theta}_1+\dot{\theta}_2)l_2\cos(\theta_1+\theta_2) + (\dot{\theta}_1+\dot{\theta}_2+\dot{\theta}_3)a_3\cos(\theta_1+\theta_2+\theta_3). \tag{7}$$

As $U_m$ and $u$ are perpendicular, as shown in Fig. 5(a), the value of $U$ can be calculated by Eq. (8). The calculation of attack angle is introduced in Fig. 5(b).

$$U^2 = U_m^2 + u^2. \tag{8}$$

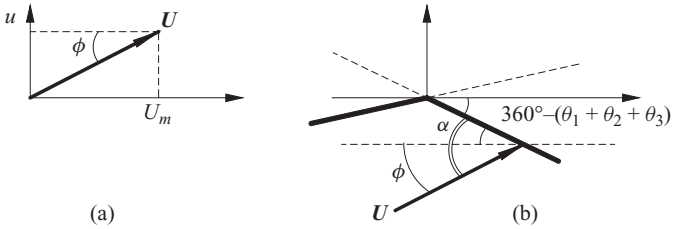



Fig. 5. (a) Relationship between $U$ and $U_m$. (b) Calculation of attack angle $\alpha$.

By using Lagrange's method, the dynamic model of the fish robot can be described briefly as shown in Eq. (9).

$$\begin{bmatrix} M_{11} & M_{12} & M_{13} \\ M_{21} & M_{22} & M_{23} \\ M_{31} & M_{32} & M_{33} \end{bmatrix} \begin{bmatrix} \ddot{\theta}_1 \\ \ddot{\theta}_2 \\ \ddot{\theta}_3 \end{bmatrix} = \begin{bmatrix} N_1 \\ N_2 \\ N_3 \end{bmatrix}. \tag{9}$$

By solving Eq. (9), we can determine the value of $\theta_i$ and $\dot{\theta}_i$ $(i = 1 \div 3)$. However, when solving the dynamic model as expressed by Eq. (9) in the simulation program, the SVD algorithm is also used in order to minimize the divergence of the fish robot's link positions in each sampling time when simulating the operation of a fish robot in an underwater environment. This divergence also causes the system to halt or else the swimming gait of the fish robot is not smooth. The calculations of $M_{ij}$ and $N_i$ $(i, j = 1 \div 3)$ are shown in the Appendix.

The motion equation of a fish robot is expressed by Eq. (10). $\ddot{x}_G$ is the acceleration of fish robot's centroid position, and $m$ is the total weight of fish robot in water ($m = 11.45$ kg). $F_F$ is the propulsion force necessary to push the fish robot forward, and $F_D$ is the drag force caused by the friction between the fish robot and the surrounding environment as the fish robot swims.

$$m\ddot{\vec{x}}_G = \vec{F}_F - \vec{F}_D. \tag{10}$$

The calculation of $F_D$ is presented in Eq. (11)

$$F_D = \frac{1}{2}\rho V^2 C_D S, \tag{11}$$

where $\rho$ is the mass density of water, $V$is the velocity of fish robot relative to water flow, and $C_D$ is drag coefficient. As

https://doi.org/10.1017/S0263574711000555 Published online by Cambridge University Press

the head of a fish robot is supposed to be of cone shape, the value of $C_D$ is assumed to be 0.5 in the simulation program. Besides, the skin of our fish robot is not smooth due to rough silicon painting, which may increase coefficient in real experiment.

$S$ is the area of the main body of the fish robot, which is projected on a plane perpendicular to the flow ($S = 0.021\,m^2$).

## 3. Fish Robot Smooth Gait Optimization Method

The optimization of a fish robot's smooth gait is presented in this section. First, we briefly discuss GA and HCA and explain why we used a combination of GA and HCA to solve this problem. Second, we address some optimal algorithms. Finally, we prove the effectiveness of the proposed method by presenting simulation results.

### *3.1. Genetic algorithm (GA) and hill climbing algorithm (HCA)*

Based on Darwin's theory of evolution, the Genetic Algorithm[18–19] starts with a set of potential populations with multiple individuals and then changes them over several iterations. The first potential population is generated or selected randomly. Each individual in the population is called a chromosome. These chromosomes evolve over several iterations, called generations. GA uses the concept of survival of the fittest by randomly initializing a population of individuals, in which each individual contains the parameters to become a possible solution to an optimization problem. Each individual in the population is assigned a fitness value that is used to indicate the quality of the individual as an optimal solution for the problem. The selected individuals then become parents on the basis of their fitness value and continue to create the next generation of potential solutions to the optimization problem. The new potential generations are generated through crossover and mutation. Sometimes the result of GA is just the local optimum, rather than the global optimal solution. In general, it is sometimes very difficult to find the real global optimal solution for a problem so that optimization by HCA will find the "near" global optimal solution for the problem. In such a case we use HCA to optimize the results of GA to improve the result. Optimization by HCA will lead to the "near" global optimal solution for the problem. There are two typical types of combination between GA and HCA. They are HCA–GA and GA–HCA. In theory, the first combination of two algorithms gives worse result than the second one. So the second type of combination is used in this paper to optimize smooth gait of our fish robot. HCA[20–21] is one of the most effective methods for an optimization problem, especially in overcoming the local optimum of a problem.

### *3.2. Using the combination of GA–HCA to get optimal parameters for fish robot's smooth gait*

A fish robot has two active joints, joint 1 and joint 2, which generate the robot's movement. $T_1$ and $T_2$ are calculated in Eqs. (12) and (13):

$$T_1 = A_1 \sin(2\pi f_1 t) \quad \text{(Nm)}, \tag{12}$$

$$T_2 = A_2 \sin(2\pi f_2 t - \beta) \quad \text{(Nm)}, \tag{13}$$

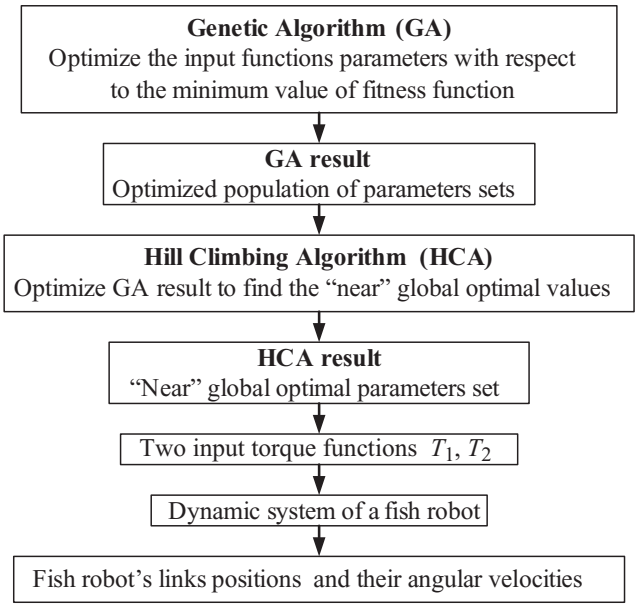



Fig. 6. Algorithm of the optimization process.

where

$A_1$, $A_2$: amplitude of the input torques for motor 1 and motor 2 (in Nm),
$f_1$, $f_2$: frequency of the input torques for motor 1 and motor 2 (in Hz),
$\beta$: phase difference between input torques of two motors (in radians).

From Eqs. (12) and (13), there are five parameters ($A_1$, $A_2$, $f_1$, $f_2$, $\beta$) that need to be optimized to build two input torque functions, $T_1$ and $T_2$, for the system. The set of optimal parameters will make the optimal input torque functions. These optimal input torque functions will allow fish robot to swim with a smooth gait, like that of a real fish.

The algorithm diagram of the optimal problem is introduced in Fig. 6.

In GA and HCA, the fitness function is used to evaluate the most suitable parameters for the system. The main objective of the fitness function for GA and HCA is to minimize the maximum increment value of $\Delta\theta_i$ for each sampling time from $t_1$ to $t_n$. The algorithm of this fitness function is based on the dynamic model of a fish robot, and it is used to check the suitability of these parameters for a fish robot. The algorithm of the fitness function is expressed in Fig. 7.

The value of $\theta_{i\ \text{Amplitude}}$ ($i = 1 \div 2$) is calculated by using Eq. (14),

$$\theta_{i\ \text{Amplitude}} = \frac{|\text{Max extremum}\,\theta_i|_t + |\text{Min extremum}\,\theta_i|_t}{2} \qquad (t_1 \le t \le t_n). \tag{14}$$

The role of HCA is to find the set of "near" global optimal parameters, which is based on the set of populations of parameters generated by GA and the fitness function. The HCA algorithm is shown in Fig. 8.

In order to use the optimization method created by GA–HCA, the five constraints of the optimized parameters must

https://doi.org/10.1017/S0263574711000555 Published online by Cambridge University Press

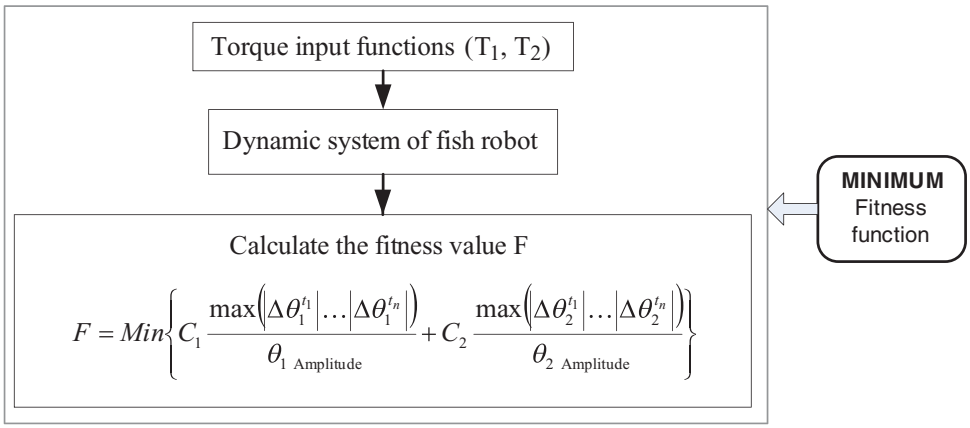



Fig. 7. Fitness function of GA and HCA.

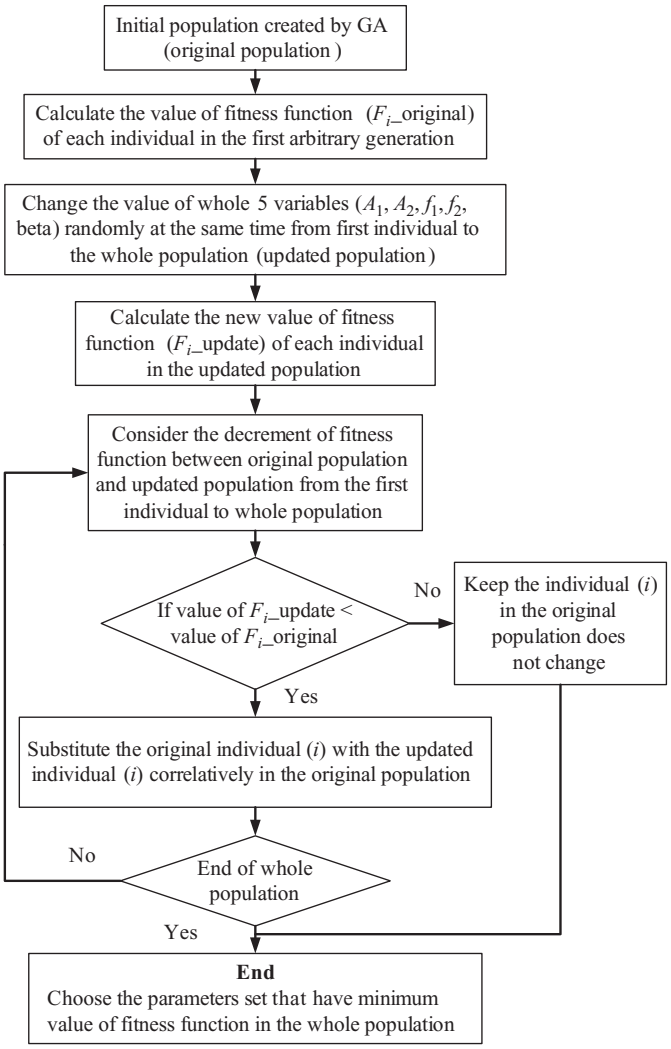



Fig. 8. HCA diagram.

be met as expressed in Eq. (15):

$$\begin{aligned} &1.\ 0 \le A_1 \le 6,\\ &2.\ 0 \le A_2 \le 6,\\ &3.\ 0 \le f_1 \le 2,\\ &4.\ 0 \le f_2 \le 2,\\ &5.\ 0 \le \beta \le \frac{\pi}{3}. \end{aligned} \tag{15}$$

If the result of GA is optimal, it will produce similar values over many subsequent generations. Once this is recognized, the GA algorithm will produce the stop condition for the optimization process.

### *3.3. GA–HCA implementation*

The simulations in this paper are carried out by using the GA toolbox of the Matlab program.[22] The GA simulation program runs with a population of 300 and 500 generations. During the heredity process, we use normalized geometric selection as a selection method, multi-nonuniform mutations as a mutation method, and arithmetic crossover as a crossover method. The optimal population generated by GA will then be optimized according to HCA to ensure that the final set of optimal parameters is the "near" global optimal set for the system.

Generally, it is very difficult to determine the most suitable values for the whole set of five parameters, $A_1$, $A_2$, $f_1$, $f_2$, $\beta$, which is based on their range values, as expressed in Eq. (15), to build two input torque functions for the system. However, this method is not ideal because if one of the values in the set is unsuitable, the input torque functions will force the system to halt or diverge. Therefore, by using the GA–HCA algorithm, combinations of five parameters, $A_1$, $A_2$, $f_1$, $f_2$, $\beta$, are chosen and evaluated suitably to ensure that their values will make the fish robot swim with a smooth gait.

## 4. Simulation Results

In this optimization method, the optimal value of five parameters ($A_1$, $A_2$, $f_1$, $f_2$, $\beta$) will be generated by GA–HCA simultaneously, according to each parameter's range of values as shown in Eq. (15). The input torque functions developed by these optimal parameters will allow fish robot to swim with a smooth gait or smooth motion. In this optimization program, two cases of input torque functions must be considered. The first case is the optimization of five parameters ($A_1$, $A_2$, $f_1$, $f_2$, $\beta$), which is called the different-frequency case ($f_1 \neq f_2$). The second case is the optimization of four parameters ($A_1$, $A_2$, $f$, $\beta$), which is called the same-frequencies case($f = f_1 = f_2$). The simulation results in each case are expressed by two typical

https://doi.org/10.1017/S0263574711000555 Published online by Cambridge University Press

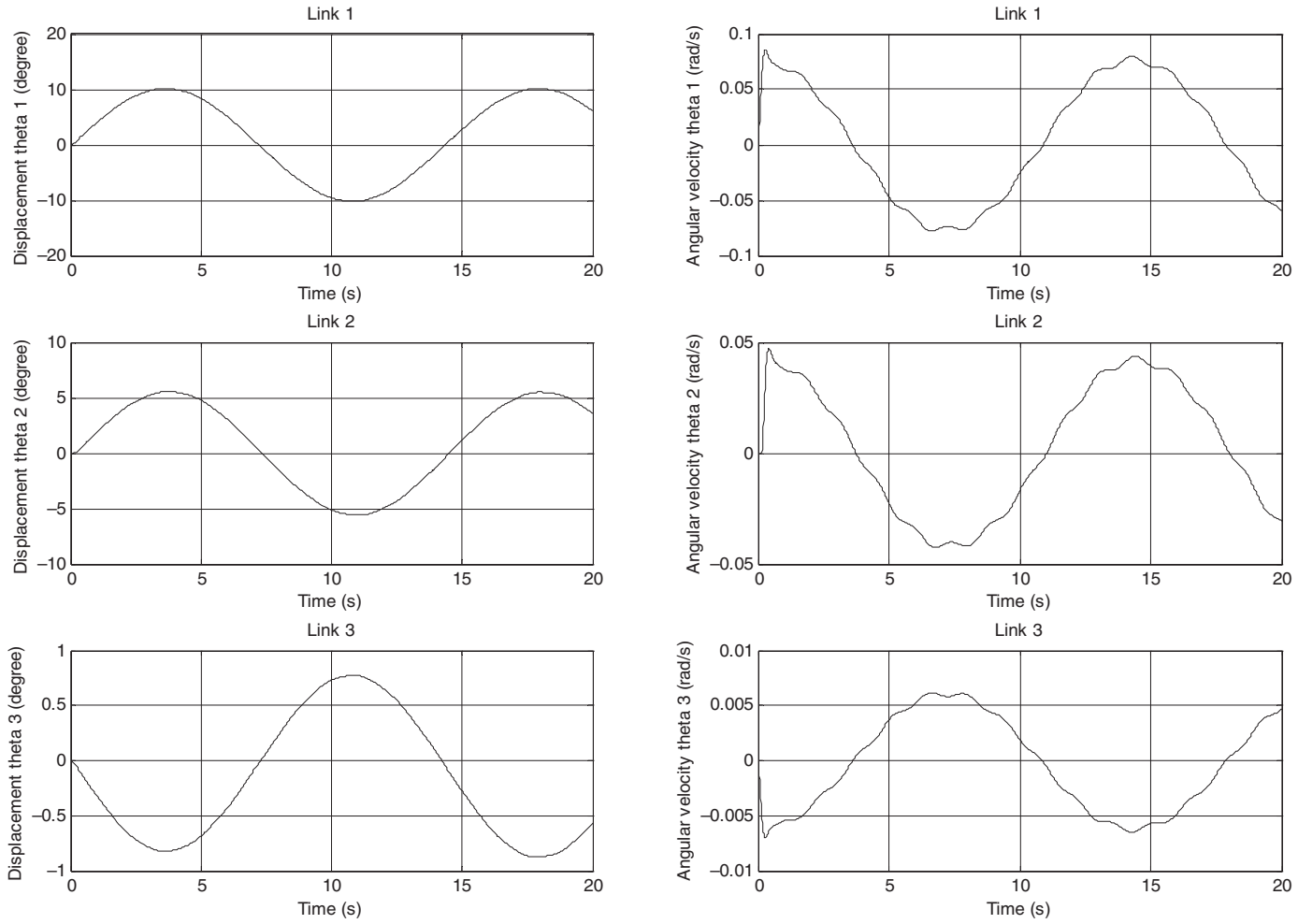



Fig. 9. Simulation of oscillations and the angular velocities of fish robot's links using Eq. (16).

examples, the optimal result and an arbitrary result, in order to prove the effectiveness of the proposed optimization algorithm.

### *4.1. Different frequencies of $f_1$ and $f_2$*

*4.1.1. Optimal case.* As GA is similar to a stochastic process, it will produce significantly different results for each runtime. However, if the result is the real optimal solution for the problem, the result will be repeated in many runtimes of GA because its fitness value is the smallest.

The two input torque functions for the system are introduced as per Eq. (16):

$$\begin{aligned} T_1 &= 3.4\sin(2\pi^*0.07t), \\ T_2 &= 0.03\sin(2\pi^*0.71t - 0.61). \end{aligned} \tag{16}$$

By applying two input torque functions given in Eq. (16) to the dynamic model of a fish robot, its average velocity was about 0.073 m/s, which was determined using Eq. (10) for an operation time of 20 s. Figure 9 simulates the operation of a fish robot's link system and the angular velocity of the links during the operation time.

The frequency of a fish robot's links, when applying the input torque functions given in Eq. (16) to the system, is about 0.07 Hz for link 1, link 2, and link 3. Smooth gait of the fish robot was evaluated according to the position of the links during each 1-s sampling period, as expressed in Fig. 10. As shown in Fig. 10, the motion of a fish robot's links and the transition of its link positions between two consecutive sampling times are smooth and regular. There is no big jump or big displacement in the links between two consecutive positions during the operation time. The initial positions of these links are marked by the horizontal line at $y = 0$.

In order to demonstrate smooth motion of a fish robot's links more clearly, the normalization method is applied to the data position of a fish robot as expressed in Eq. (17):

$$\begin{aligned} \theta_i &= \left[\theta_i^{t1} \ldots \theta_i^{tn}\right]^T, \quad i = 1 \div 3, \\ \hat{\theta}_i &= \frac{\theta_i^{tk}}{\sqrt{\sum_{k=1}^{n}\left(\theta_i^{tk}\right)^2}}. \end{aligned} \tag{17}$$

By applying the normalization method, the expression of the fish robot's link displacement for each sampling time from the beginning to the ending is introduced in Fig. 11, where the position of the fish robot's link distribution during the operation time is very smooth. The circles in the curves in Fig. 11 are the expressions of $\text{link}_i (i = 1 \div 3)$ positions for each sampling time of 1 s. The changing state from the

https://doi.org/10.1017/S0263574711000555 Published online by Cambridge University Press

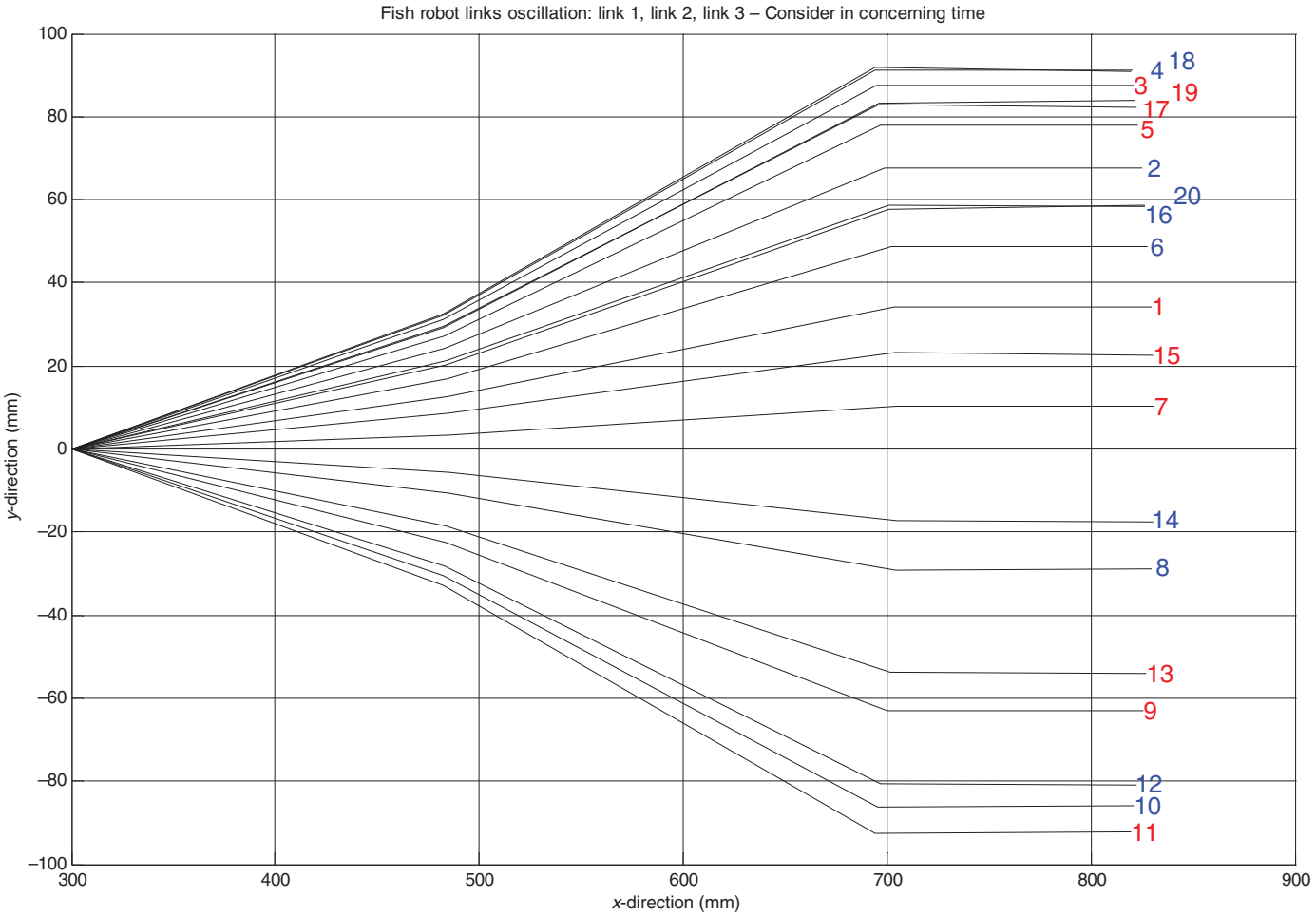



Fig. 10. (Colour online) Fish robot's link position for each sampling interval of 1 s during the operation time as calculated using Eq. (16).

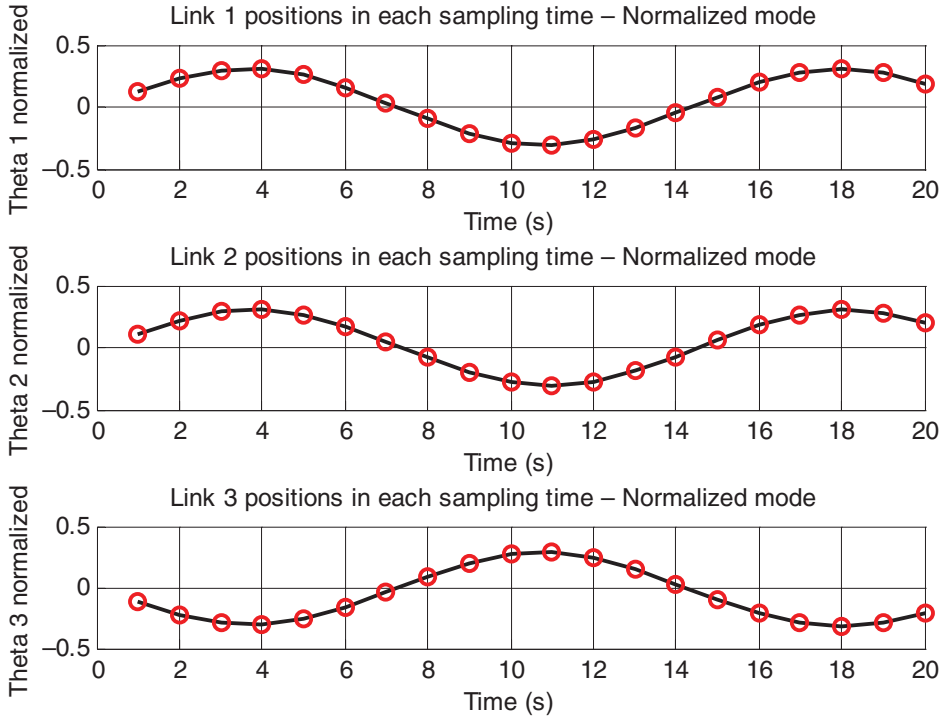



Fig. 11. (Colour online) Fish robot's link positions for each sampling time of 1 s by applying Eq. (16) and the normalization method.

https://doi.org/10.1017/S0263574711000555 Published online by Cambridge University Press

Table I. Optimal value of parameters in different-frequency case.

| No. | $A_1$ | $A_2$ | $f_1$ | $f_2$ | Beta ($\beta$) | Fitness value |
|---|---|---|---|---|---|---|
| 1. | 3.40 | 0.03 | 0.07 | 0.71 | 0.61 | 17 |

Table II. Arbitrary value of parameters set in different-frequency case.

| No. | $A_1$ | $A_2$ | $f_1$ | $f_2$ | Beta ($\beta$) |
|---|---|---|---|---|---|
| 1. | 3.83 | 1.36 | 0.07 | 0.71 | 0.64 |

current position to the next position for each sampling time is very smooth. The displacement or the gap of each step position is regular, and there is no big jump from the current position at time $t_i$ to the next position at time $t_{I+1}$ for the entire operation time of 20 s.

The fitness value, which is equal to 17 in Table I, expresses the "worth" or the "value" of the parameters set in Table I. This fitness value is evaluated by GA. For example, if there are other parameter sets whose fitness values are bigger than 17, then they are worse than the parameter set in Table I. This means that when we use a new set of parameters to create the input torque functions for the system, the new performance of the system is worse than the ordinary performance of the system, which the input torque function produces from the parameter set in Table I. In other words, the parameter set in Table I is the optimal set of parameters, which generates a smooth gait for a fish robot in the different-frequency case. This fitness value's characteristic is similar in the same-frequency case.

*4.1.2. Arbitrary case or non-optimal case.* In the arbitrary case or the non-optimal case, the value of each parameter, which is used to build the input torque functions in the system, is chosen arbitrarily on the basis of the range of values for each parameter as in Eq. (15). As shown in Table II, we choose the same-frequency of arbitrary case as the frequencies of optimal case in order to prove the effectiveness of the proposed algorithm.

When the values of amplitudes and phase differences are chosen in arbitrary case, the response of the system is not good. This means that the fish robot does not have the smooth motion when we choose arbitrary or non-optimal parameters set as input torque functions. This tendency is also observed when the robot is tested with arbitrary parameters set for the same frequencies case.

The two input torque functions for the system are introduced as in Eq. (18):

$$\begin{aligned} T_1 &= 3.83\sin(2\pi^*0.07t), \\ T_2 &= 1.36\sin(2\pi^*0.71t - 0.64). \end{aligned} \tag{18}$$

Similar to the optimal case, by applying the two input torque functions given in Eq. (18) to the dynamic model of a fish robot, the average velocity of the fish robot is about 0.18 m/s for 20 s. Figure 12 simulates the operation of a fish robot's link system and its angular velocity during the operation time. As this is an arbitrary case, the performance of the fish robot's link oscillation and their angular velocities are worse than the performance of those in an optimal case. From Fig. 12, the oscillations of a fish robot's links and their angular velocities are not stable. In general, the amplitudes of the links' oscillations and their angular velocities do not remain stable during the operation time. In the arbitrary case, the fish robot's link frequencies are higher than those in the optimal case. The frequency values of the three links from link 1 to link 3 are about 0.6 Hz.

As this case is an arbitrary one, there will be big jumps or big gaps between each step from sampling time $t_i$ to $t_{i+1}$ of the fish robot's link positions as expressed in Figs. 13 and 14.

In Fig. 13, there are some big jumps in the position of the fish robot's links at certain sampling times. In the normalization mode, the links' positions are not smooth between the current and the next step as shown in Fig. 14. The displacements between the current position of the links at the current time $t_i$ and the next position at the next time $t_{i+1}$ are considerably large and irregular.

In order to show the effectiveness of the proposed method, a comparison of fish robot's link positions in one cycle between the optimal case and the arbitrary case is presented in Fig. 15.

In Fig. 15, the performance of the fish robot's links in the optimal case is smoother than that in the arbitrary case, and there is no big increment or big decrement of the links' positions for each sampling interval during the operation time. The transition positions from the current position to the next position are very smooth and regular in the optimal case.

So according to simulation results, if we put the optimal input torque functions into the system, the fish robot will swim with a smooth gait or smooth motion, similar to a real fish.

### *4.2. Same frequencies of $f_1$ and $f_2$*

*4.2.1. Optimal case.* Similarly to the optimal case of different frequencies, the optimal set of parameters in the same-frequency case is also obtained by using the simulation results of GA–HCA, as shown in Table III.

Table III. Optimal value of parameters in same-frequency case.

| No. | $A_1$ | $A_2$ | $f = f_1 = f_2$ | Beta ($\beta$) | Fitness value |
|---|---|---|---|---|---|
| 1. | 2.78 | 0.94 | 0.08 | 0.05 | 10.08 |

The two input torque functions for the system are introduced as in Eq. (19):

$$\begin{aligned} T_1 &= 2.78\sin(2\pi^*0.08t), \\ T_2 &= 0.94\sin(2\pi^*0.08t - 0.05). \end{aligned} \tag{19}$$

By applying Eq. (19) to the system, the average velocity of the fish robot is about 0.074 m/s, and the value of the fish robot's link frequencies is about 0.08 Hz for link 1, link 2,

https://doi.org/10.1017/S0263574711000555 Published online by Cambridge University Press

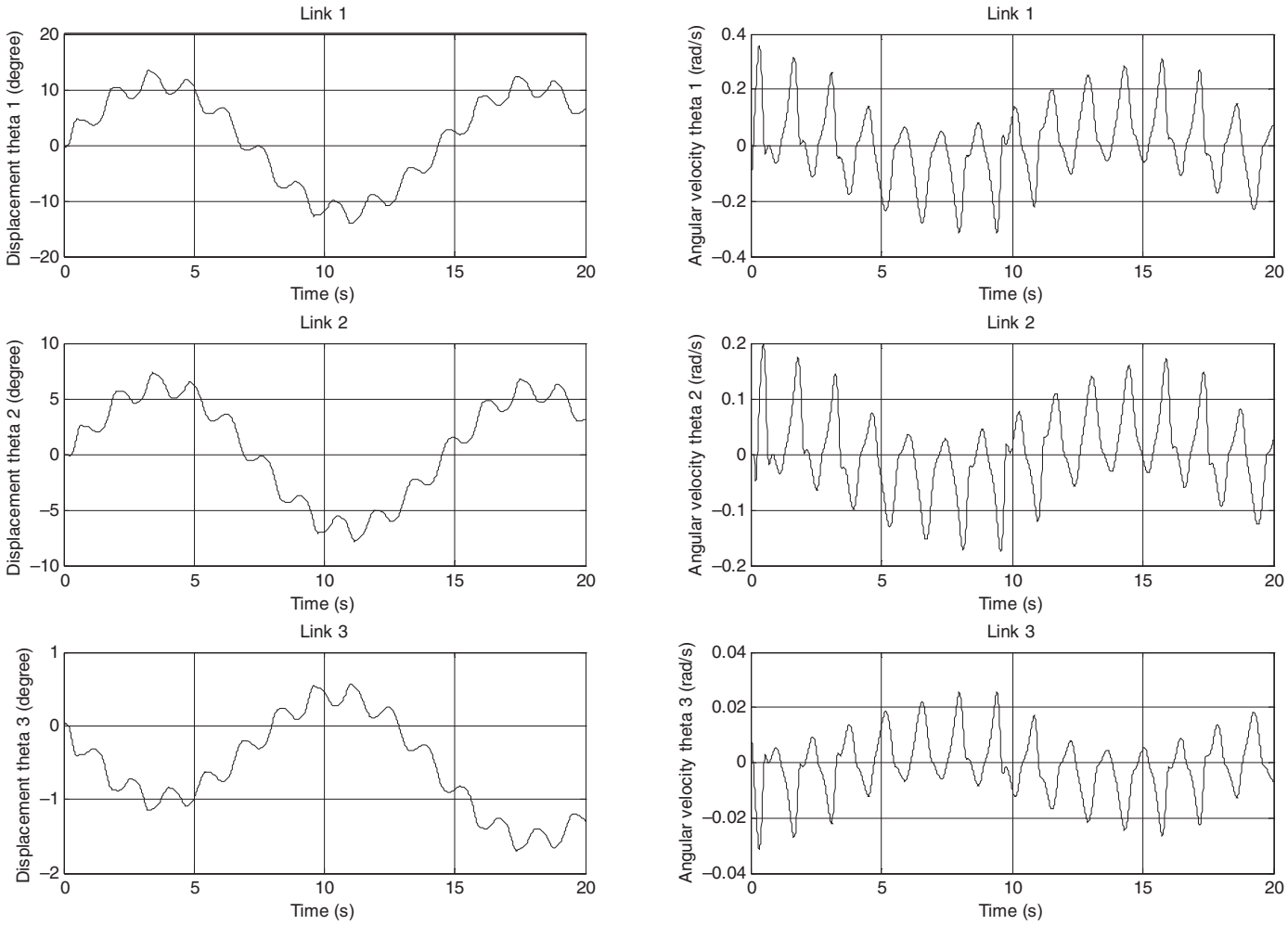



Fig. 12. Simulation of fish robot's link oscillations and their angular velocities by using Eq. (18).

and link 3. The performance of these links' oscillations and their angular velocities are presented in Fig. 16.

As the input torque functions in the system are optimal, the fish robot's link movements are very smooth and stable as seen in Figs. 17 and 18. In addition, the performances of the links' angular velocities are very smooth as seen in Fig. 16. This means that by using these optimal input torque functions, the fish robot will swim with a smooth gait during the operation time.

As with the positions resulting from a set of optimal parameters in the different-frequency case, the positions of the fish robot's links are considered for each 1-s sampling period. As seen in Figs. 17 and 18, the transition positions of these links among the sampling times are very smooth and regular. There is no big jump from the current position to the next position for each link's oscillation during concerning time.

The circles in the curves in Fig. 18 are the expression of $\text{link}_i (i = 1 \div 3)$ positions for each 1-s sampling period during the operation time.

*4.2.2. Arbitrary or non-optimal case.* Similarly to the arbitrary case of the different-frequency situation, the value of each parameter used to create two input torque functions in the system is chosen randomly as in Table IV according to their range value as in Eq. (15).

The two input torque functions for the system are introduced as in Eq. (20):

$$\begin{aligned} T_1 &= 2.26 \sin(2\pi^{*}0.08t), \\ T_2 &= 3.05 \sin(2\pi^{*}0.08t - 1.03). \end{aligned} \tag{20}$$

By applying Eq. (20) to the dynamic system of the fish robot, the average value of velocity after 20 s is about 0.07 m/s, and the value of the fish robot's link frequencies is about 0.08 Hz for link 1, link 2, and link 3. The performance of the fish robot's link oscillations and their angular velocities are introduced as shown in Fig. 19. As these are arbitrary parameters, when we apply the input torque functions created by these parameters to the system, the performance of the fish robot's link oscillations and their angular velocities or the transition between each sampling period from the current position to the next one are not as smooth as that in the optimal case, as shown in Figs. 19–21. In Fig. 19, the link motions of the fish robot are not smooth in the beginning, and the motion tends to be shifted into a positive region during the remaining time. This means that fish robot's links do not oscillate around the center position and their angular velocities are not smooth. Therefore, fish robot does not swim in smooth motion when we use arbitrary parameters set to build the input functions.

https://doi.org/10.1017/S0263574711000555 Published online by Cambridge University Press

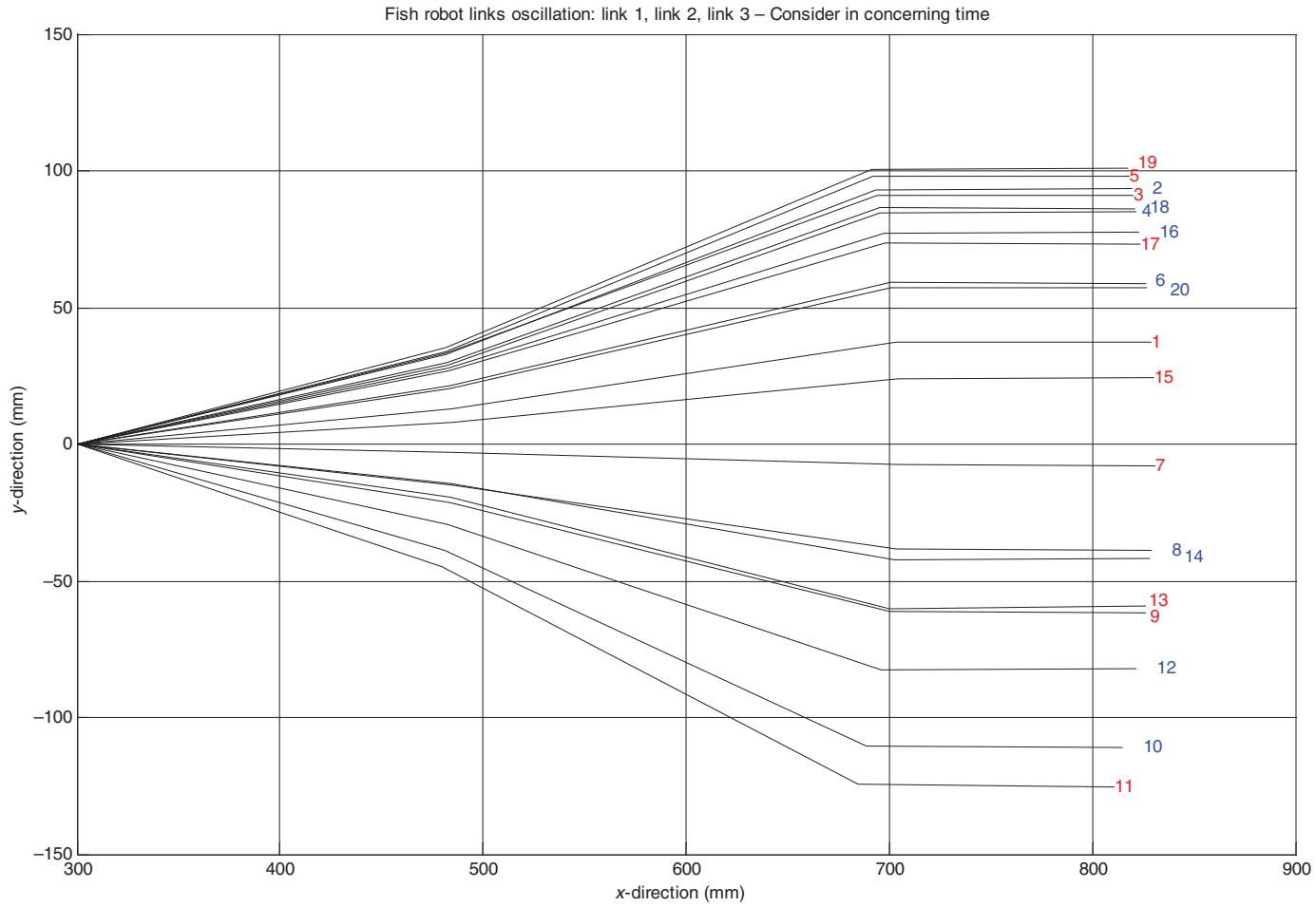



Fig. 13. (Colour online) Fish robot's link position for each sampling interval of 1 s during the operation time as calculated using Eq. (18).

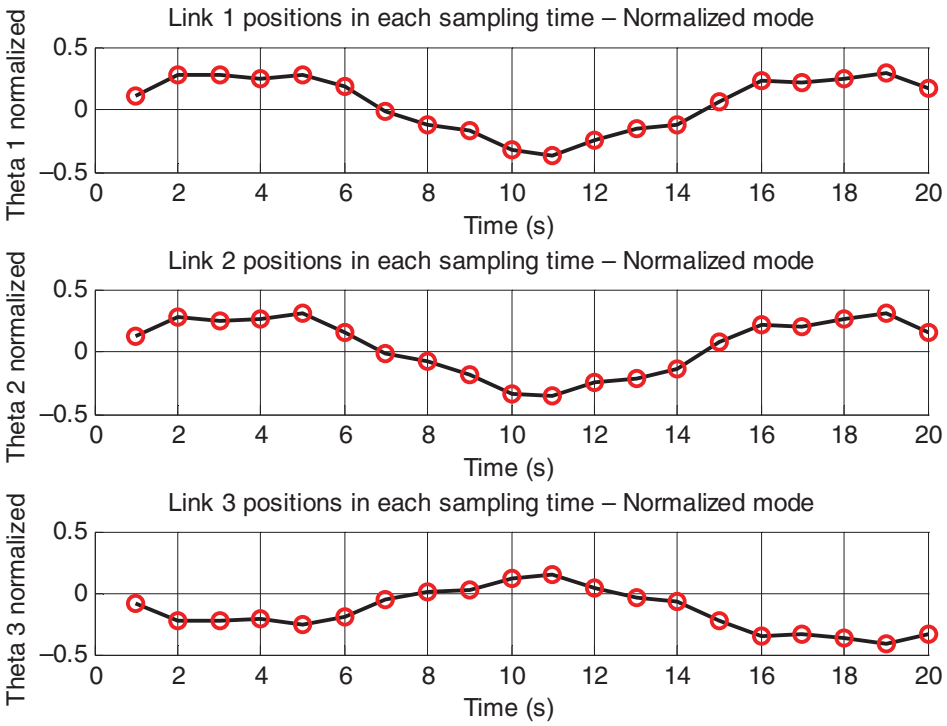



Fig. 14. (Colour online) Fish robot's link positions for each sampling interval of 1 s determined by applying Eq. (18) and the normalization method.

https://doi.org/10.1017/S0263574711000555 Published online by Cambridge University Press

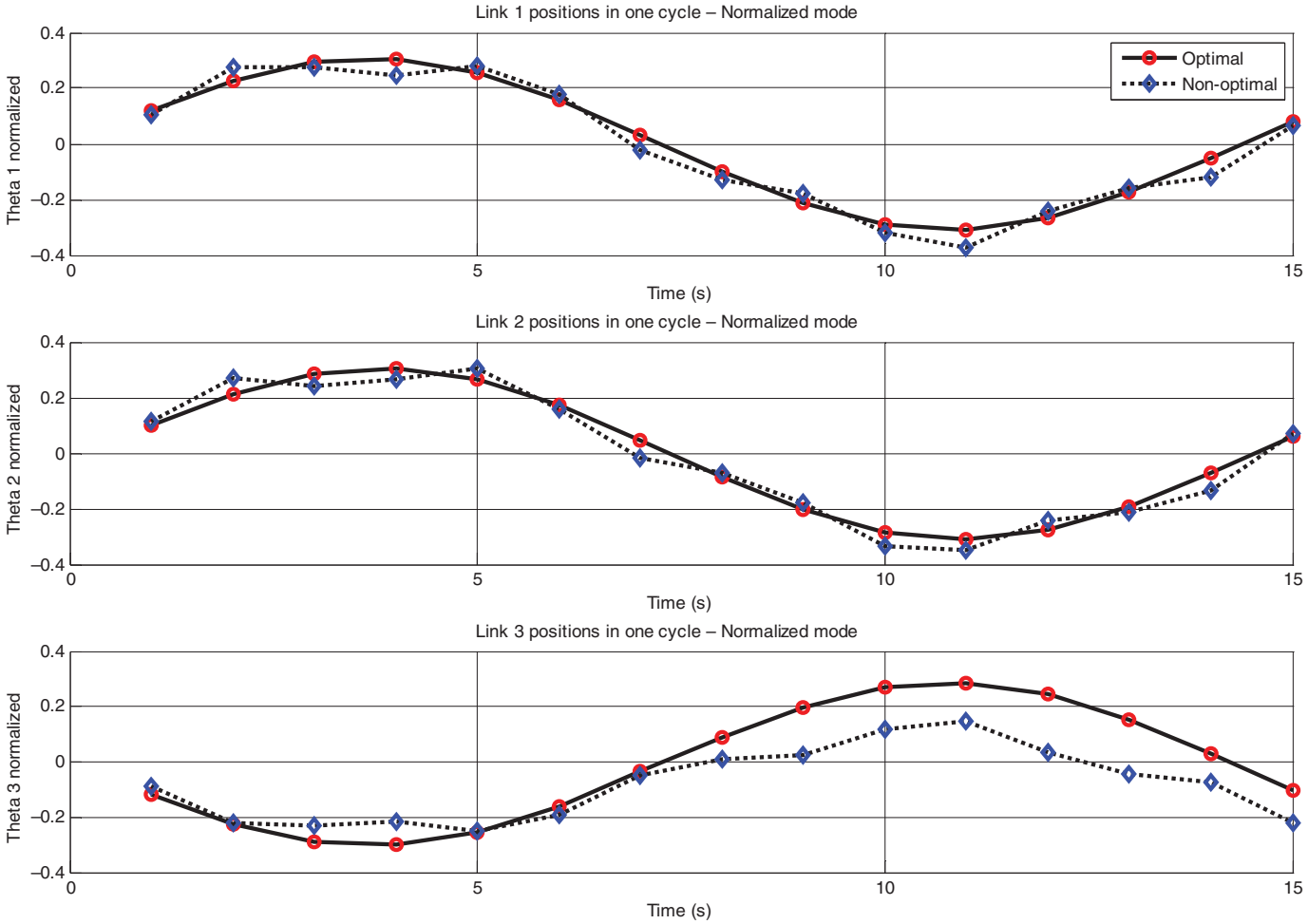



Fig. 15. (Colour online) Comparison of the links' positions in the normalization mode between optimal case and arbitrary case for one cycle.

Table IV. Values of the set of arbitrary parameters in same-frequency case.

| No. | $A_1$ | $A_2$ | $f = f_1 = f_2$ | Beta ($\beta$) |
|---|---|---|---|---|
| 1. | 2.26 | 3.05 | 0.08 | 1.03 |

There are some big jumps between certain sampling time points, and the transition positions of the links at the current time $t_i$ to the next time $t_{i+1}$ during the operation time are not smooth as seen in Fig. 20. The transition positions of fish robot's links at some sampling times are not regular. Besides, the fish robot's links have a trend to be shifted into the positive region as seen in Fig. 21.

By comparing the optimal and arbitrary parameters in this case, we demonstrate the effectiveness of the proposed method. This means that by using the optimization method of GA–HCA, the movement of the fish robot is reliable with a smooth gait or smooth motion, similarly to a real fish.

Figure 22 introduces the positions of a fish robot's links for one cycle time when we apply the optimal and arbitrary input torque functions to the dynamic system of a fish robot. As with the different-frequency case, the optimal parameters in this case make the fish robot swim with a smoother gait than with the arbitrary parameters. The transition positions from the current sampling time to the next sampling time of the optimal case are very smooth and regular, and there is no big jump in the links' positions between two consecutive sampling times without any link shift.

In summary, by comparing two cases with different and same frequencies, the optimal parameters in each case produce a better result than the arbitrary case. The input torque functions created by the set of optimal parameters will make the fish robot swim with a smooth gait or smooth motion during the operation time. In addition, in the optimal case, the transition positions of the fish robot's links for each sampling time are very smooth. From the current position to the next position in each sampling time of 1 s for the optimal case, the displacements among the sampling times are quite regular. This means that there is no sudden increment or sudden decrement of the links' displacement for each sampling period during the operation time. With the optimal parameters set generated by using the combination of GA–HCA, the motion of the fish robot is guaranteed to have a smooth gait or smooth motion like that of a real fish during swimming. It is not only the optimal input torque functions that create smoother movement for the fish robot's links as indicated by comparing Fig. 15 and Fig. 22 but also the performance of angular velocities in the optimal case are better than that in the arbitrary case. This can be seen by

https://doi.org/10.1017/S0263574711000555 Published online by Cambridge University Press

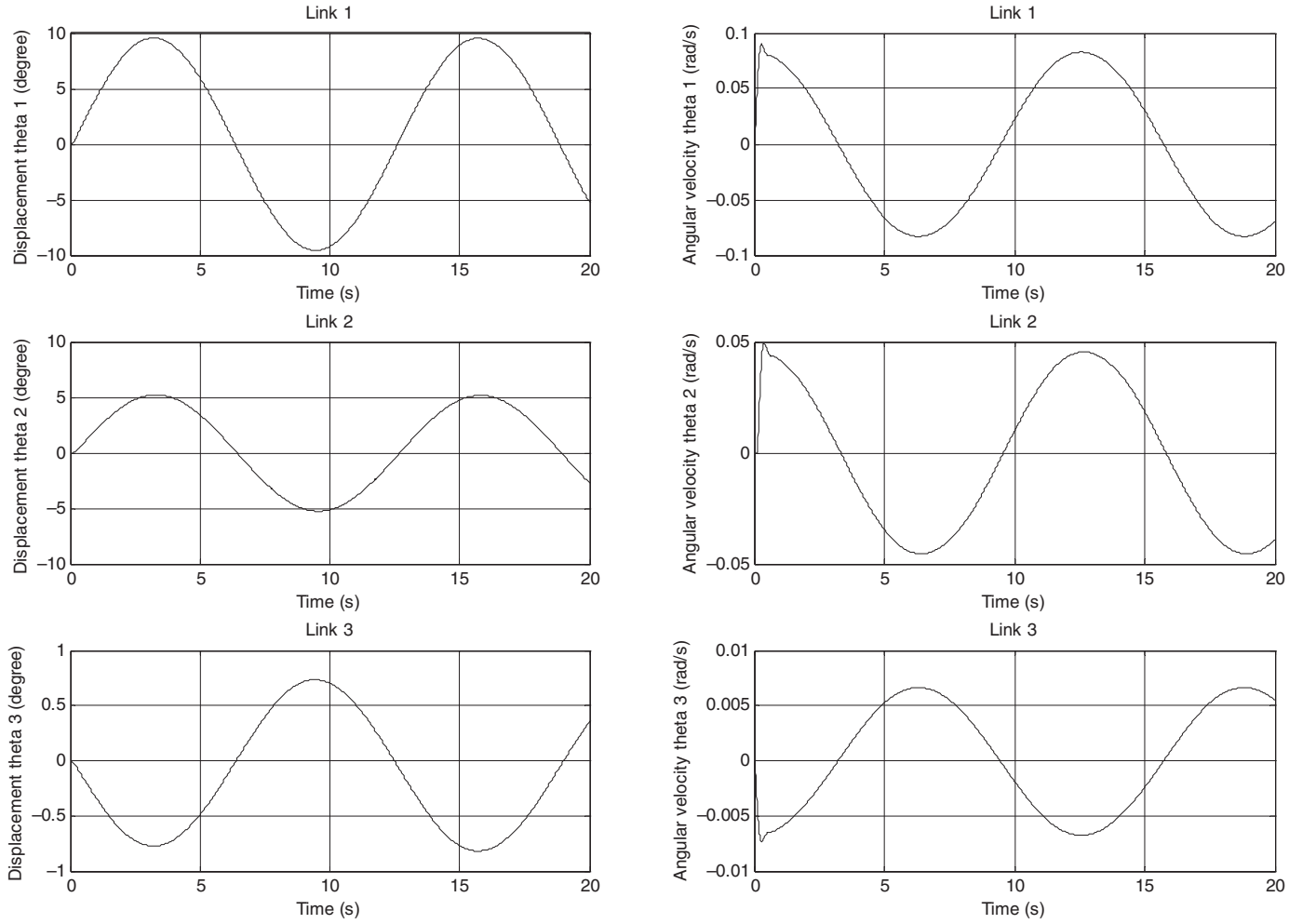



Fig. 16. Simulation of fish robot's link oscillations and their angular velocities by using Eq. (19).

comparing Fig. 9 and Fig. 12 for the different-frequency case or Fig. 16 and Fig. 19 for the same-frequency case.

Generally, in our proposed method the optimal result is achieved by using the combination of GA–HCA. As proven by the simulation results, the proposed method produces a good swimming gait for a fish robot. Indeed, the optimal set of parameters will make a fish robot swim with a smooth gait or smooth motion like that of a real fish.

## 5. Experimental Results

In order to prove the feasibility of the proposed algorithm in this paper, some essential experiments are carried out by using a fish robot that is developed in the laboratory.

Figure 23 is a photograph to describe the internal structure of a fish robot such as joints, links, and controller boxes. Figure 24 shows its external appearance painted with silicon.

In our research, we consider a fish robot with a total length of about 1200 mm, which includes four links. The head and body of a fish robot are considered to be one rigid part (link 0), which is connected to link 1 by joint 1. Link 1 and link 2 are then connected by joint 2. These links and joints are shown in Fig. 2. Each joint includes an active motor and a beveled gearbox. The equivalent stiffness values of these gearboxes are 5.13 Nm/rad at joint 1 and 4.95 Nm/rad at joint 2. Finally, link 3 (lunate tail fin) is connected to link 2 with joint 3 by two extension flexible springs to imitate smooth motion of a real fish. The stiffness value of each spring is about 100 N/m. The lengths of link 1, link 2, and link 3 are 245 mm, 160 mm, and 127 mm, respectively. The introduction to a fish robot's physical parameters is briefly summarized in Table V.

Table V. Fish robot parameters.

| | Link 1 | Link 2 | Link 3 (tail fin) |
|---|---|---|---|
| Mass (kg) | 1.4 | 0.45 | 0.2 |
| Moment of inertia (kg $m^2$) | 0.016 | $7.26 * 10^{-3}$ | $1.307 * 10^{-3}$ |
| Length of link (m) | 0.185 | 0.22 | 0.126 |
| Center of gravity (m) | 0.093 | 0.11 | 0.063 |
| Spring stiffness (N/m) | 5.13 | 4.95 | 100 |
| Forming parts | | Styrofoam | |
| Skin | | Silicon | |

The data recording process for the experimenting fish robot is carried out as shown in Fig. 25.

The main controller that is used to control two active DC servo motors at two joints (joint 1, joint 2) of a fish robot as introduced in Fig. 23 is the ATmega128 micro controller. This micro controller will generate the control

https://doi.org/10.1017/S0263574711000555 Published online by Cambridge University Press

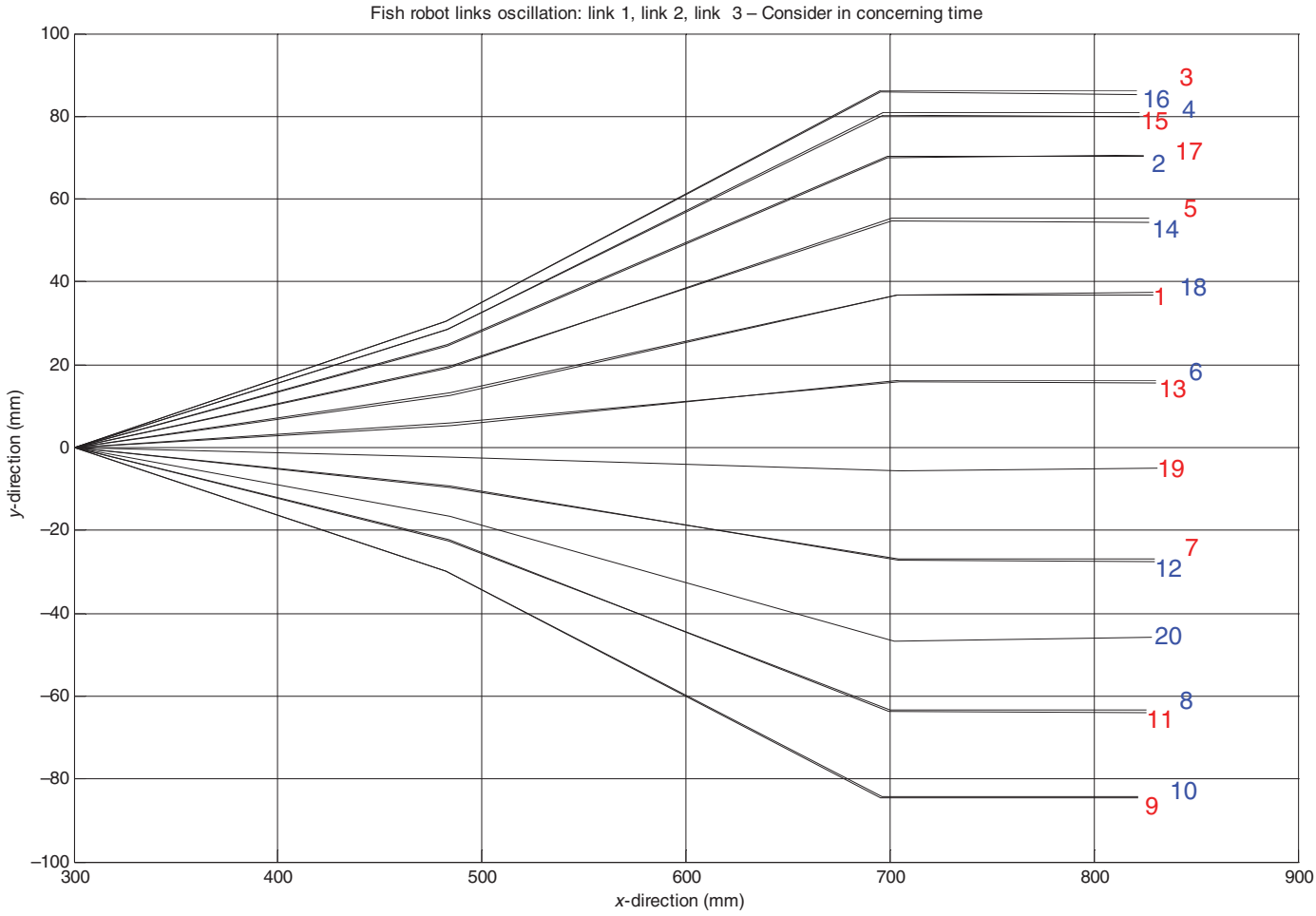



Fig. 17. (Colour online) Fish robot's link position for each sampling period of 1 s during the operation time by using Eq. (19).

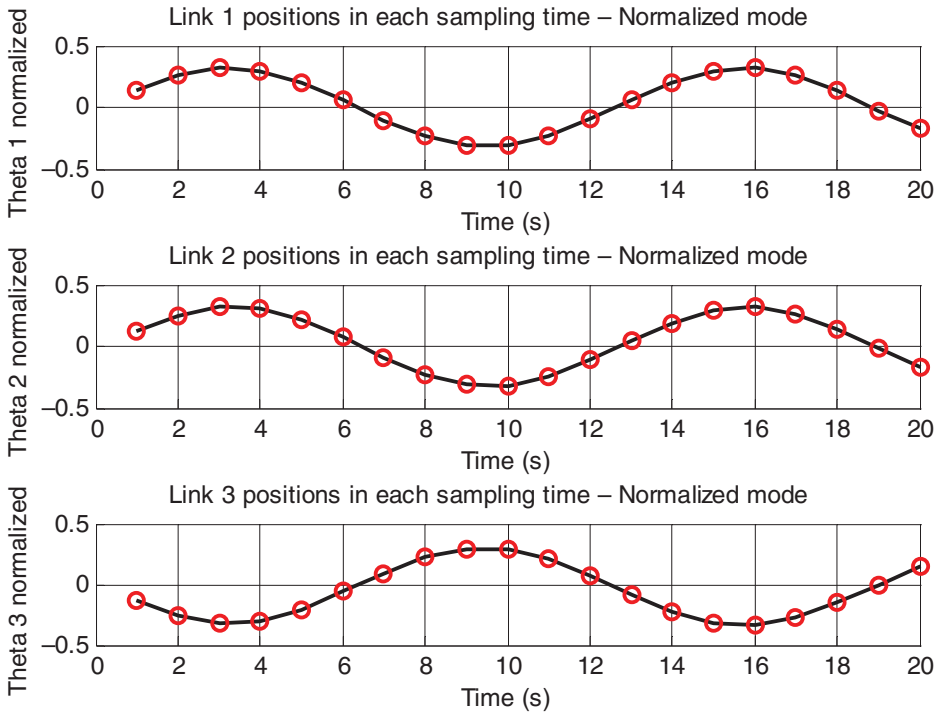



Fig. 18. (Colour online) Fish robot's link positions for each sampling time of 1 s by applying Eq. (19) and the normalization method.

https://doi.org/10.1017/S0263574711000555 Published online by Cambridge University Press

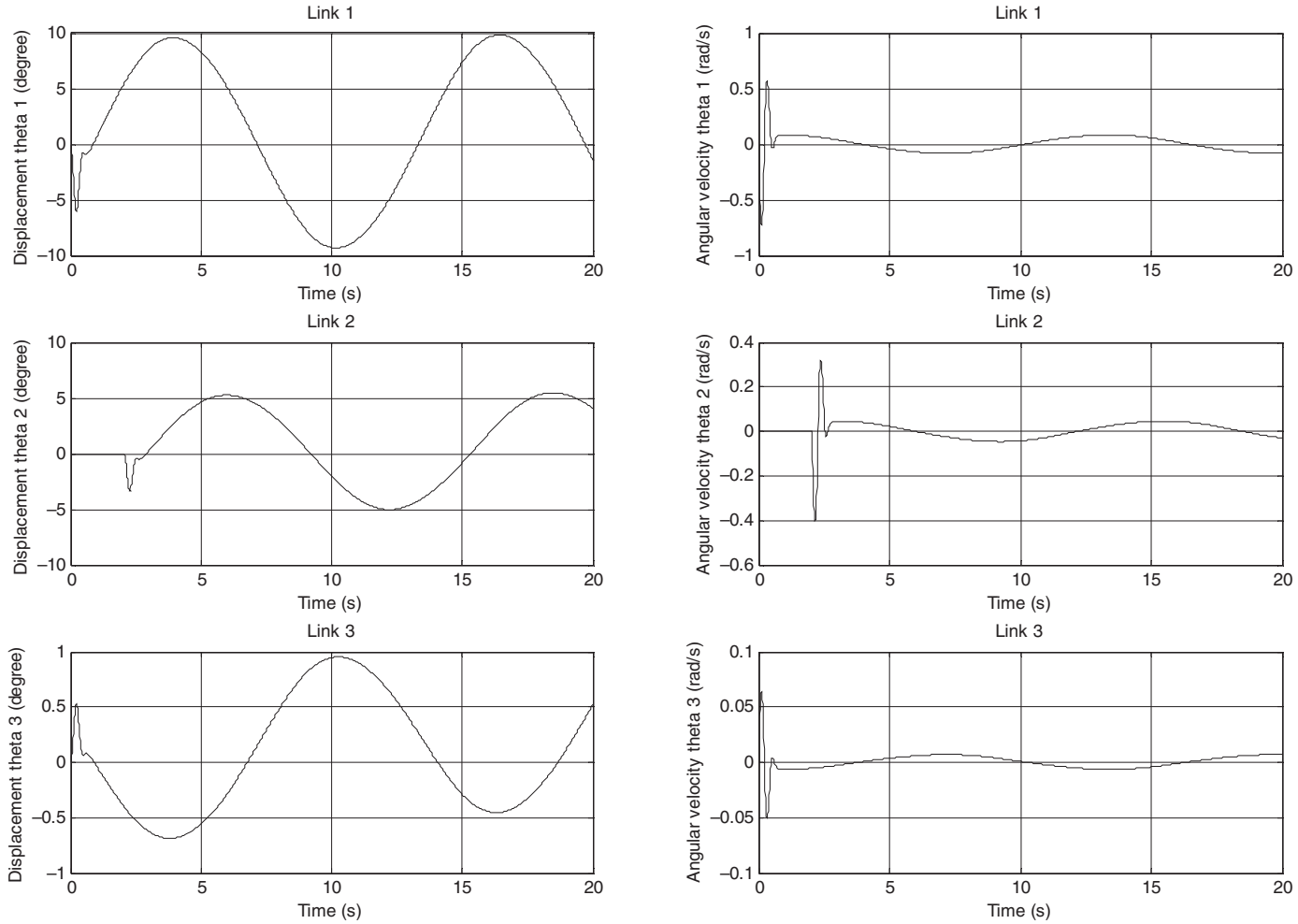



Fig. 19. Simulation of fish robot's link oscillations and their angular velocities by using Eq. (20).

signal to these motors. Fish robot is tested in water tanks (160 cm × 90 cm × 60 cm). The signals of two quadrature encoders at two DC servomotors are linked to a computer via two channels of Advantech PCI-1784 card. The experimental processes are carried out with two types of input torque functions, which are the different-frequency and same-frequency cases.

Due to both limitation of the fish robot's mechanical structure and some not-so-good experimental conditions in the simulation, there is little difference between the simulation and experimental results. However, the experiment proved that the concept of optimal input torque function would make fish robot swim with a smooth motion or smooth gait. Therefore, considering this concept, the experimental results are said to agree with the simulation results. Some requisite experimental results are introduced in the following part.

### *5.1. Different frequencies of $f_1$ and $f_2$*

*5.1.1. Optimal case.* The input torque function used in this experiment is given in Eq. (16), which introduces as the optimal input torque function for fish robot in different-frequency case.

*5.1.2. Arbitrary or non-optimal case.* The input torque function applied in this case is given in Eq. (18).

In real experiment, the oscillations of fish robot's links have little differences from the simulation. Due to the motion transmission of mechanical system inside fish robot and also the water resistance, the delay appears when fish robot's links rotate to the maximum angle and return. This means that in the real experiment as introduced in Figs. 26 and 27, the delay happens when the motors, which connect to fish robot's links, change direction of motion. Moreover, in the experiment results, the optimal cases of different frequencies make fish robot move with a smooth motion and the oscillations of fish robot's links are kept symmetrical via center position (zero degree), and also the shape of motion or the motion pattern is repeated by time as shown in Fig. 26. The keeping of motion shape shows that the transition of fish robot's links in each sampling time is graduated.

However, with the non-optimal input torque function as in Fig. 27, the oscillations of a fish robot's links are not kept symmetrical by time. This means that the peduncle part of fish robot has the trend to be shifted to one side, and the shape of motion pattern is not kept or does not repeat by time. These phenomena show that the motion of a fish robot is not smooth. The transition of links in each sampling time is also not graduated. These phenomena in non-optimal cases also agree with simulation results.

https://doi.org/10.1017/S0263574711000555 Published online by Cambridge University Press

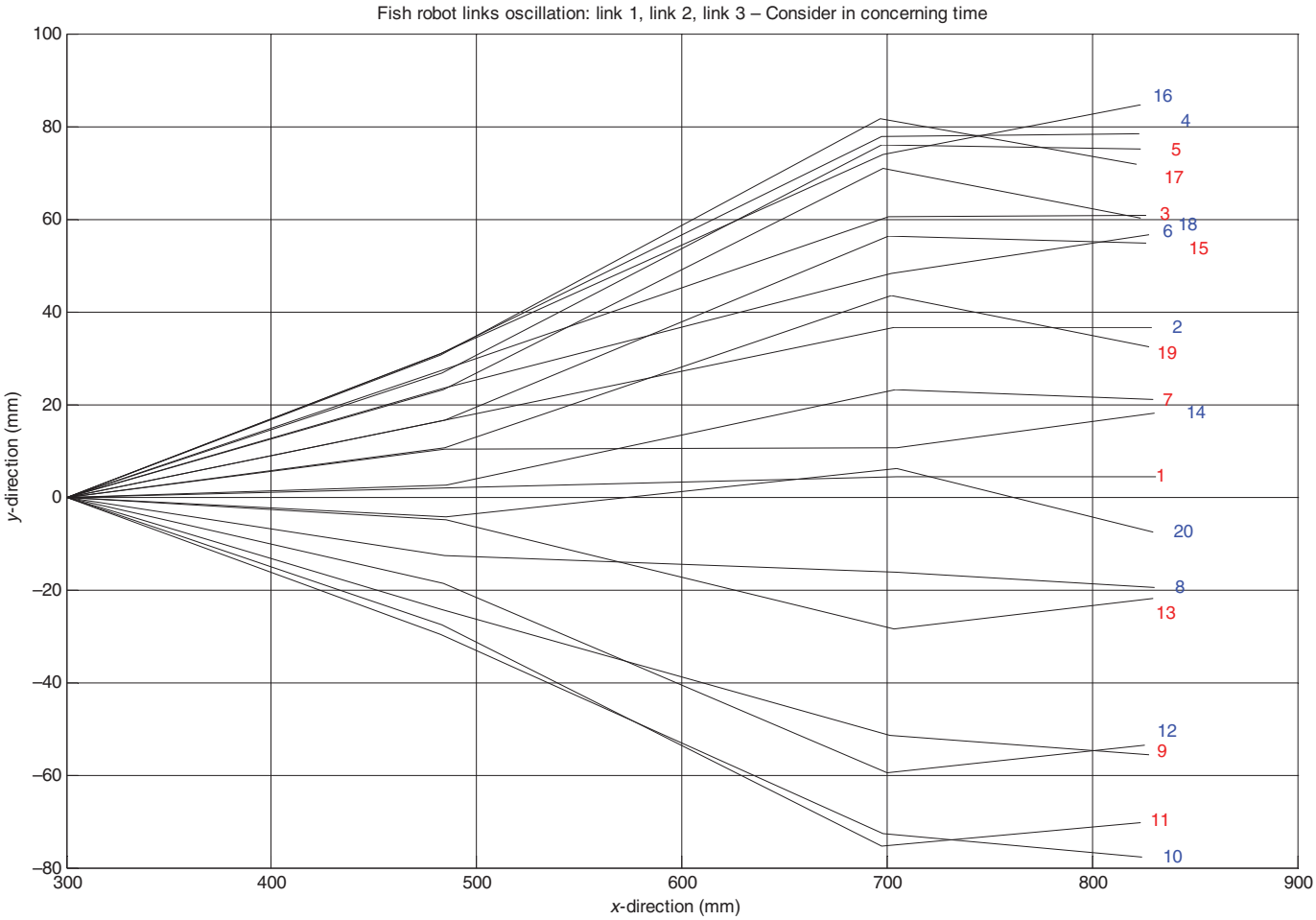



Fig. 20. (Colour online) Fish robot's link positions for each 1-s sampling period during the operation time by using Eq. (20).

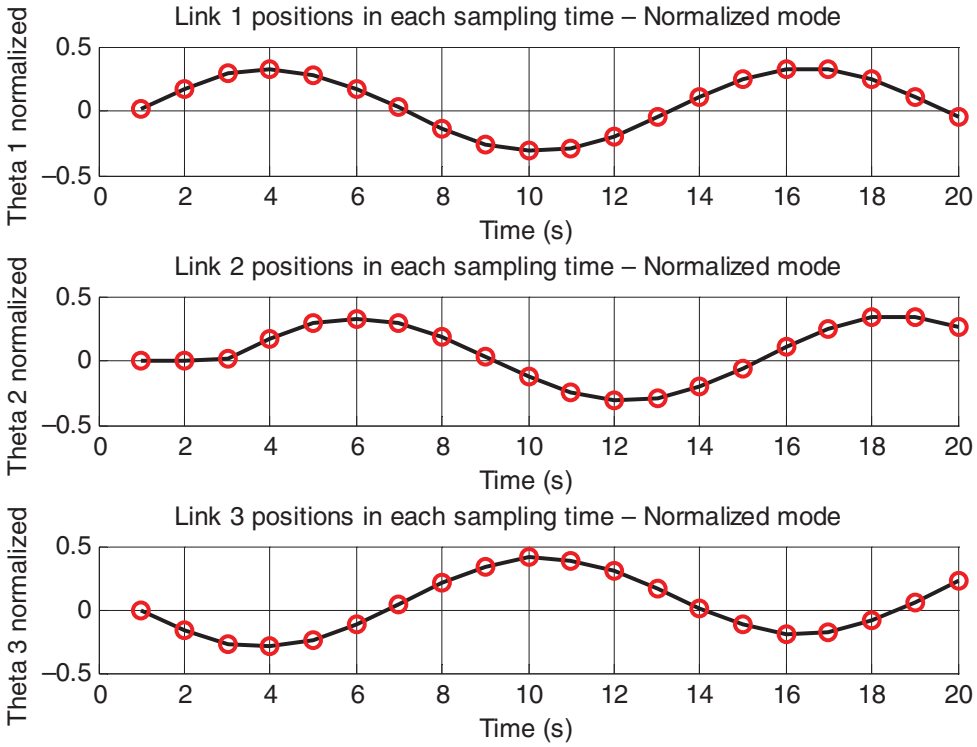



Fig. 21. (Colour online) Fish robot's link positions for each 1-s sampling period determined by applying Eq. (20) and the normalization method.

https://doi.org/10.1017/S0263574711000555 Published online by Cambridge University Press

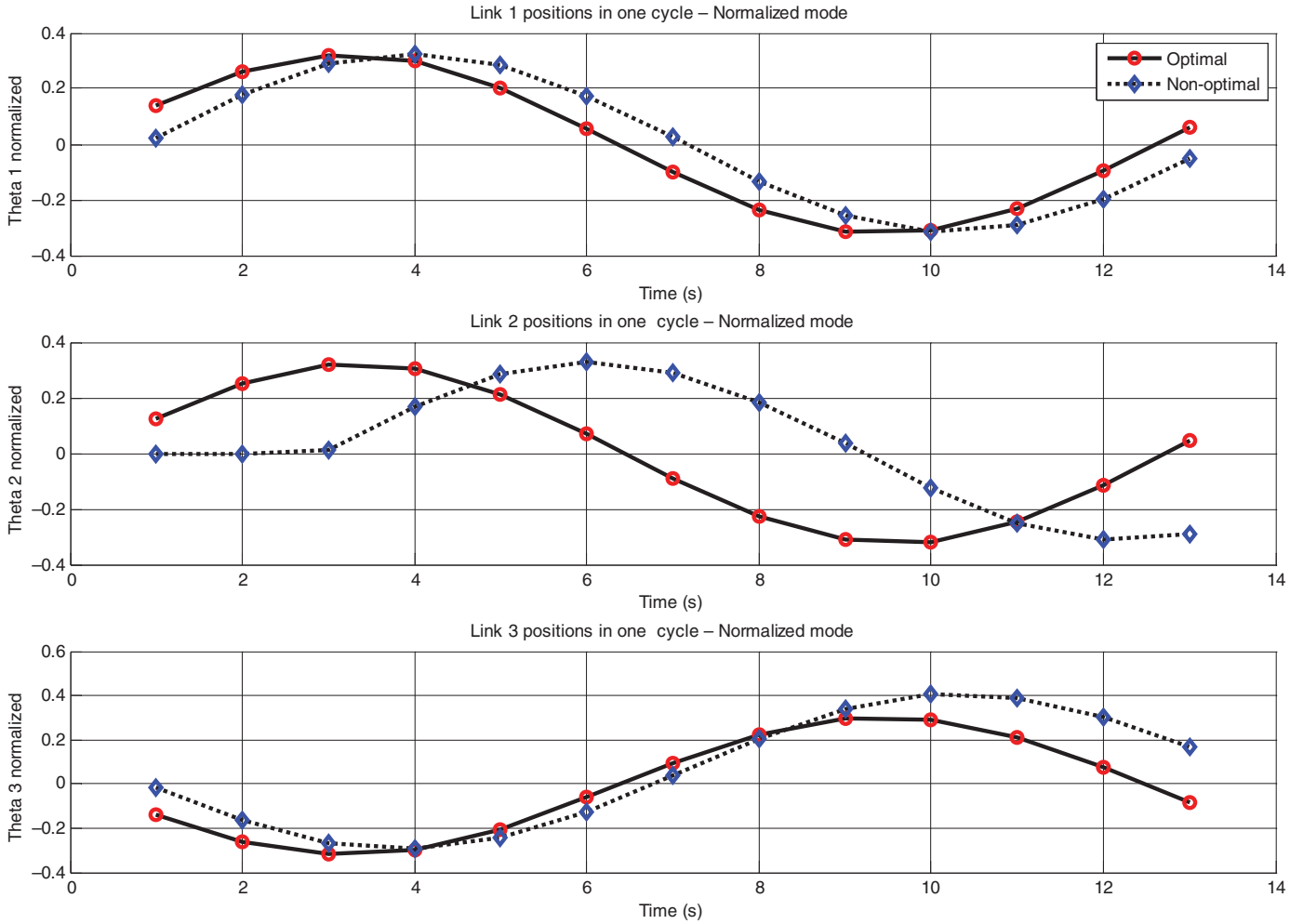



Fig. 22. (Colour online) Comparison of links' positions in the normalization mode between optimal case and arbitrary case for one cycle time.

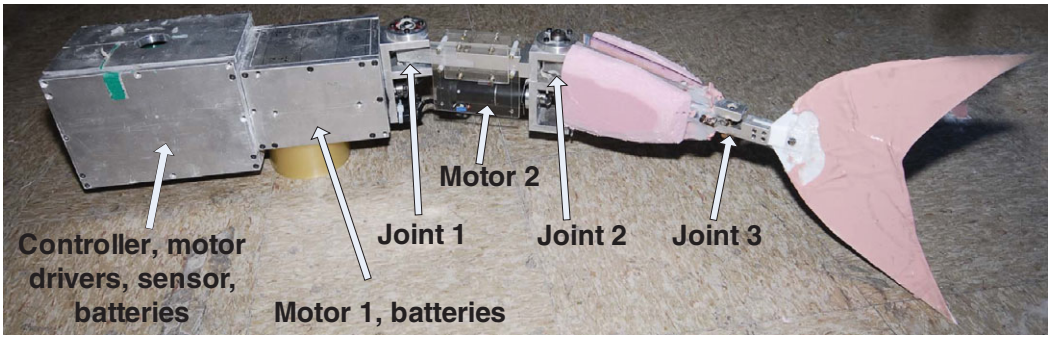



Fig. 23. (Colour online) Internal structure of a fish robot.



Fig. 24. (Colour online) Exterior shape of a fish robot.

https://doi.org/10.1017/S0263574711000555 Published online by Cambridge University Press

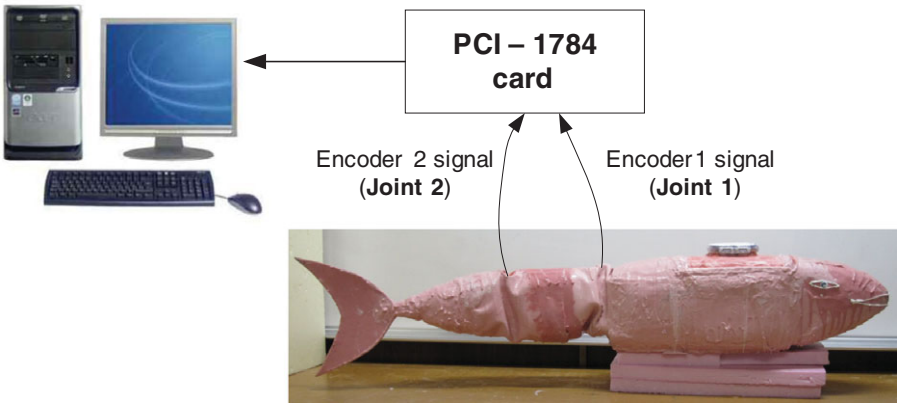



Fig. 25. (Colour online) Data recording for experiment fish robot.

In simulation results, the optimal of input torque functions will make fish robot swim with a smooth motion or smooth gait, which is better than the non-optimal of input torque function. This confirmation is proved by the experimental results. Besides, the proof of this confirmation is also introduced by Fig. 28, which shows the comparison of the experimental results between optimal and non-optimal input torque functions. The real performances of a fish robot are shown just like the simulation results shown in Fig. 15.

### 5.2. *Same frequencies of $f_1$ and $f_2$*

*5.2.1. Optimal case.* The optimal input torque function used for experimenting fish robot is given in Eq. (19). By using this optimal function to test the motion of a fish robot, the motion of a fish robot is quite smooth and also better than the optimal input torque function in different-frequency case. This also agrees with the simulation result.

In Fig. 29, there is also little difference between the simulation and the experimental results. However, the concept of smooth motion or smooth gait of a fish robot is still kept. The real motions of fish robot's links are smooth and kept symmetrical via the center position. Likewise, the motion shape is repeated by time and the shift phenomenon of a fish robot's links does not appear during the simulation time. In this case, the keeping of motion shape during the simulation time shows that the transition of fish robot's links in each sampling time is graduated. Therefore, by applying the optimal input torque functions, which are of same frequencies, the fish robot swims with a smooth gait or smooth motion.

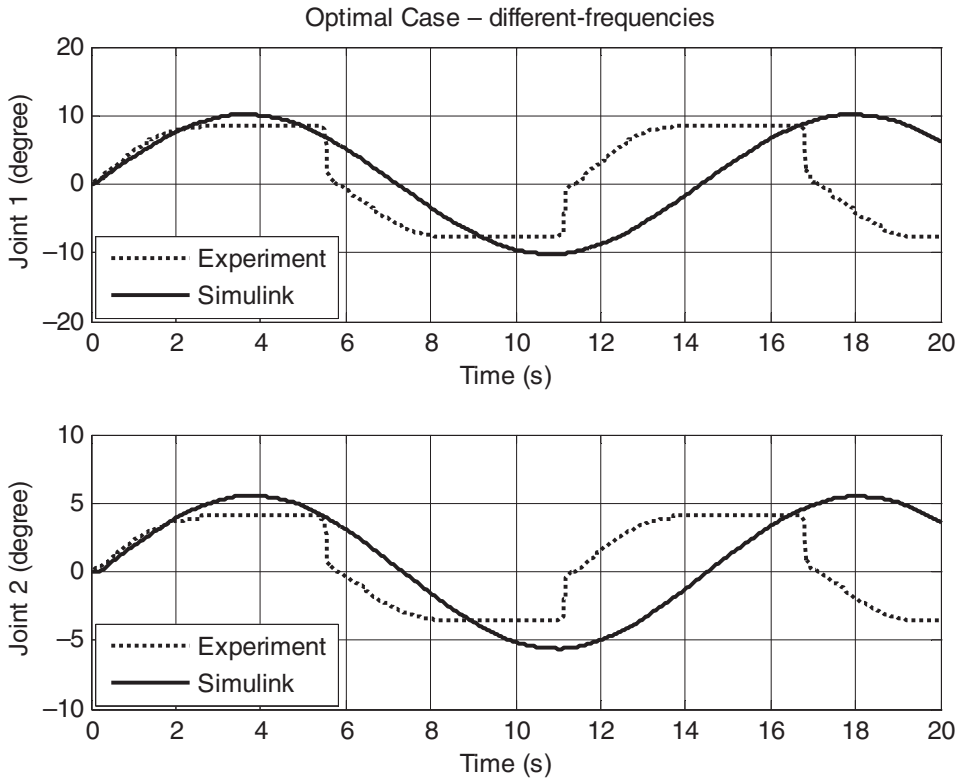



Fig. 26. Fish robot's link oscillations by experimental results when applying Eq. (16) to fish robot.

https://doi.org/10.1017/S0263574711000555 Published online by Cambridge University Press

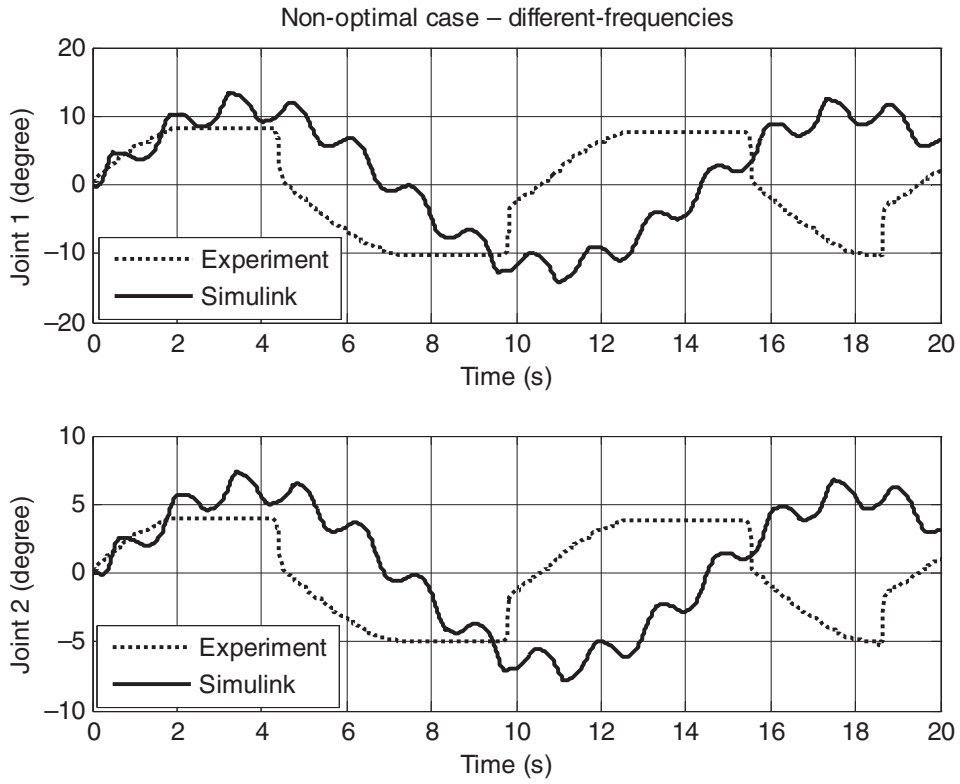



Fig. 27. Fish robot's link oscillations by experimental results when applying Eq. (18) to fish robot.

*5.2.2. Arbitrary or non-optimal case.* Similar to previous cases, Eq. (20), which is non-optimal of same-frequency case, is used to test the real performance of a fish robot. The experimental result is presented in Fig. 30.

In Fig. 30, the non-optimal input torque functions also make fish robot swim in a non-symmetric state, and the motion shape does not keep during the concerning time. The non-optimal input torque functions also do not make the oscillations of fish robot's links as smooth as the optimal input torque functions. In both simulations and experimental results, the oscillation of fish robot's links does not keep symmetrical via the center position and also the motion shape

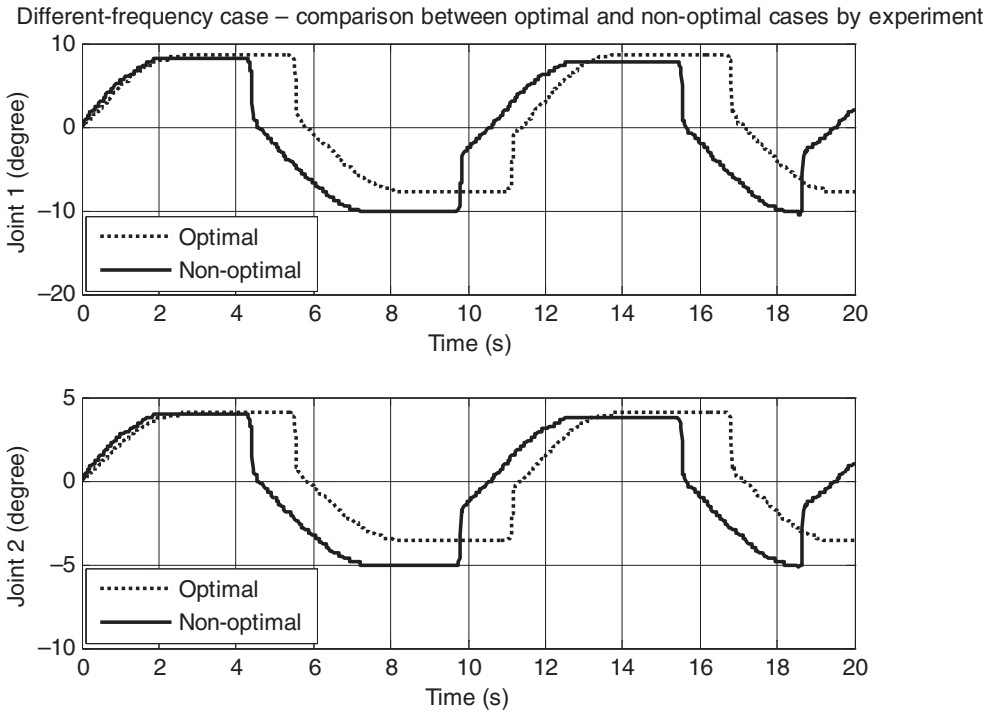



Fig. 28. Comparison of experimental results between optimal and non-optimal cases by applying Eqs. (16) and (18) to fish robot.

https://doi.org/10.1017/S0263574711000555 Published online by Cambridge University Press

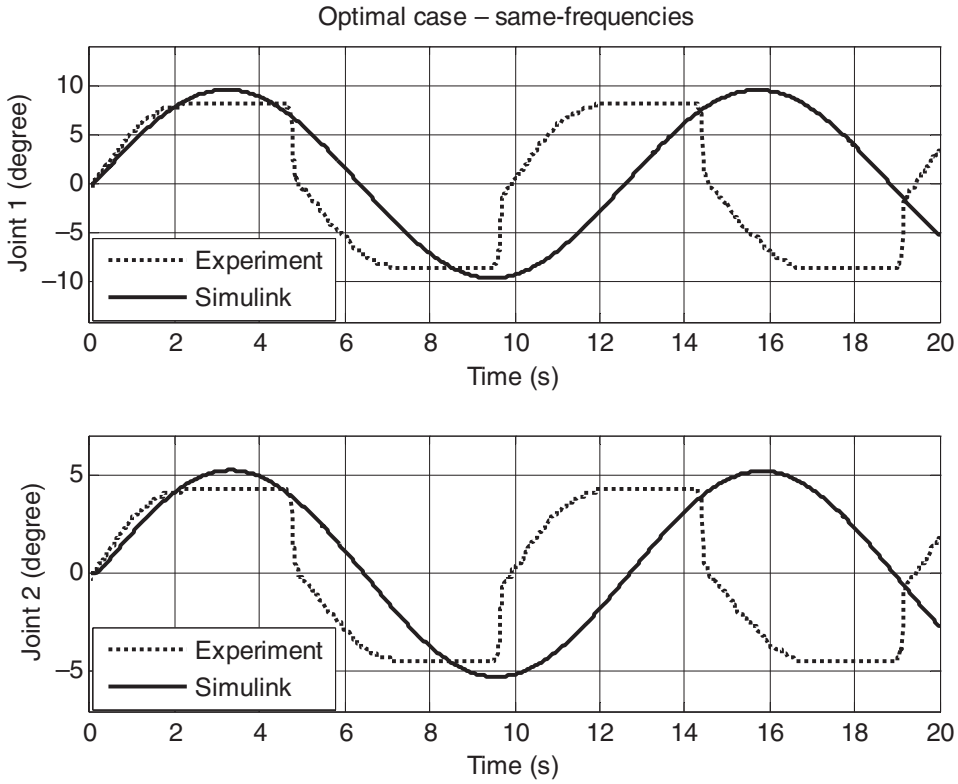



Fig. 29. Fish robot's link oscillations by experimental results when applying Eq. (19) to fish robot.

changes during the simulation time. This is an agreement between the simulation and experimental results.

Figure 31 introduces the comparison of real fish robot's link oscillation between optimal and non-optimal of input torque functions with same-frequency case. In this figure, the optimal input torque functions always make fish robot swim with smoother motion than the non-optimal input function. This concept also agrees with the

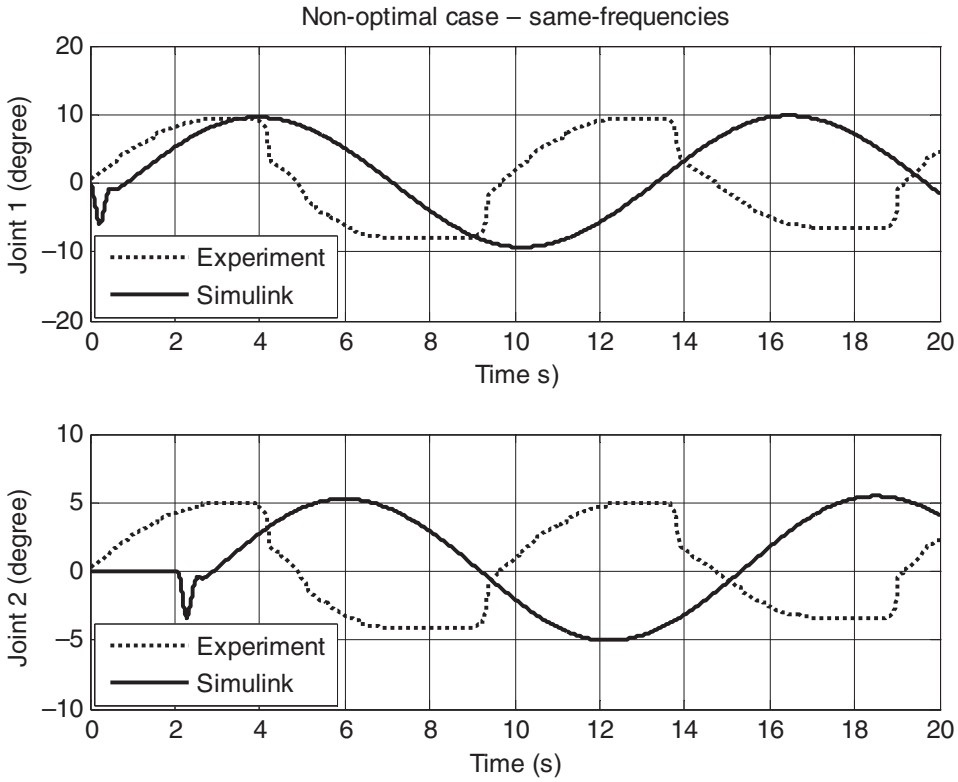



Fig. 30. Fish robot's link oscillations by experimental results when applying Eq. (20) to fish robot.

https://doi.org/10.1017/S0263574711000555 Published online by Cambridge University Press

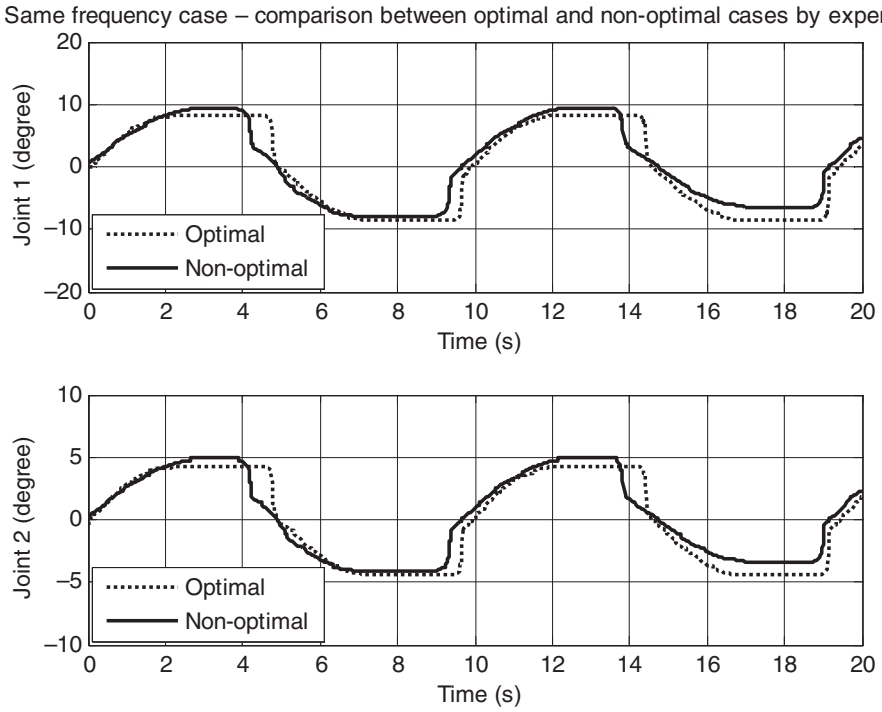



Fig. 31. Comparison of experimental results between optimal and non-optimal cases by applying Eqs. (19) and (20) to fish robot.

simulation result as expressed in Fig. 22 in the simulation part.

In summary, by comparing two cases with different and same frequencies in experimental results, the optimal parameters in each case produce a better result than the arbitrary case or the non-optimal case. The input torque functions created by a set of optimal parameters, which are optimized by the combination of GA–HCA, will make fish robot swim with a smooth gait or smooth motion during the operation time. Due to the limitation of mechanical system inside fish robot, there is little difference between the simulation and the real experimental results. However, the concept that the optimal input torque functions will make fish robot swim with a smooth gait or smooth motion is proved by experimental results. This is the agreement between the experimental and simulation results. In experimental results, the optimal input torque functions make fish robot swim with symmetrical oscillation and transition of links in each sampling time is smooth and graduated. Besides, the non-optimal input torque functions make fish robot generate the non-symmetric oscillations via the center position, and the motion patterns are not kept repeated during the simulation time. This means that the motions of a fish robot in non-optimal cases as well as the transition of links in each sampling time are not smooth. Therefore, with the optimal parameters set generated by using the combination of GA–HCA, the motion of a fish robot guarantees a smooth gait or smooth motion during swimming.

## 6. Conclusion

In this paper, a model of a 3-joint carangiform fish robot is presented. From this type of fish robot, a dynamic model is derived by using Lagrange's method. The influence of fluid force, which is exerted on the motion of a fish robot in an underwater environment, is considered in the robot's dynamic model by using the concept of Lighthill's[4] carangiform propulsion and Nakashima *et al*'s[17] concept. An SVD algorithm is used in our simulation program as an effective method for reducing the divergence of a fish robot's link motion when solving the matrix of its dynamic model.

By using the GA–HCA simulation program, the set of optimal parameters, which is determined by two input torque functions for two active motors at joint 1 and joint 2, is obtained. These two optimal input torque functions in two cases of having different and identical frequencies of $f_1$ and $f_2$, respectively, can make the fish robot swim with a smooth gait or smooth motion with respect to its dynamic model. A comparison of the set of optimal parameters generated by GA–HCA with the arbitrary set of parameters demonstrates the effectiveness of the proposed method. Besides, some primitive experiments are carried out to check the real motion of a fish robot when applying the optimal and non-optimal parameters input torque functions. The experimental results also show that the optimal parameters generated by GA–HCA make fish robot swim with a smooth gait or smooth motion, which is better than the arbitrary parameters set or the non-optimal parameters set. Therefore, with the process of proving by simulation and experiment, the effectiveness of the optimization method for fish robot's smooth gait by using the combination of GA–HCA is proposed and verified.

## 7. Future Work

In order to try to solve the smooth gait problem, we will improve the experimental conditions to obtain better results. Another application of GA will be considered in trying to solve the control problem for our fish robot. One of the most effective applications of GA in the control problem is the application of an intelligent control technique, such as a

https://doi.org/10.1017/S0263574711000555 Published online by Cambridge University Press

combination of GA and CPG, which should be considered in designing a suitable controller.

**Acknowledgment**

This work was supported by the Korean Research Foundation grant (KRF-2008-521-D00152). The authors would like to express their deep gratitude for the financial support provided by KRF.

**References**

1. C. S. Yeow and C. C. Chien, "Adaptive control schemes for autonomous underwater vehicle," *Robotica* **27**, 119–129 (2009).
2. D. McFarland, I. Gilhespy and E. Honary, "DIVEBOT: A diving robot with a whale-like buoyancy mechanism," *Robotica* **21**, 385–398 (2003).
3. G. V. Lauder and E. G. Drucker, "Morphology and experimental hydrodynamics of fish fin control surfaces," *IEEE J. Ocean. Eng.* **29**(3), 556–571 (2004, Jul.).
4. M. J. Lighthill, "Hydromechanics of aquatic animal propulsion," *Annu. Rev. Fluid Mech.* **1**, 413–446 (1969, Jan.).
5. J. Yu and L. Wang, "Parameter Optimization of Simplified Propulsive Model for Biomimetic Robot Fish," *Proceedings of the 2005 IEEE International Conference on Robotics and Automation*, Barcelona, Spain (Apr. 2005) pp. 3306–3311.
6. W. Zhao, J. Yu, Y. Fang and L. Wang, "Development of Multi-mode Biomimetic Robotic Fish Based on Central Pattern Generator," *Proceedings of the 2006 IEEE/RSJ International Conference on Intelligent Robots and Systems*, Beijing, China (Oct. 9–15, 2006) pp. 3891–3896.
7. D. B. Zhang, D. W. Hu, L. C. Sheng and H. B. Xie, "A bionic neural network for fish robot locomotion," *Sci. Direct J. Bionic Eng.* **3**, 187–194 (2006).
8. J. Liu, I. Dukes, R. Knight and H. Hu, "Development of Fish-Like Swimming Behaviours for An Autonomous Robotic Fish," *Proceedings of Control 2004*, University of Bath, Bath, UK (Sep. 6–9, 2004) pp. 1049–1054.
9. J. Yu, S. Wang and M. Tan, "A simplified propulsive model of bio-mimetic robot fish and its realization," *Robotica* **23**, 101–107 (2005).
10. M. J. Lighthill, "Note on the swimming of slender fish," *J. fluid Mech.* **9**, 305–317 (1960).
11. K. Seo, R. Murray and J. S. Lee, "Exploring Optimal Gaits For Planar Carangiform Robot Fish Locomotion," *Proceedings of the 16th IFAC World Congress*, Prague, Czech (Jul. 2005).
12. J. Guo, "A way-point tracking controller for a biomimetic autonomous underwater vehicle," *Ocean Eng.* **33**, 2369–2380 (2006).
13. J. Liu and H. Hu, "Building a Simulation Environment for Optimising Control Parameters of an Autonomous Robotic Fish," *Proceeding of the 9th Chinese Automation & Computing Society Conference*, Luton, UK (Sep. 20, 2003).
14. I. Borazjani and F. Sotiroulos, "Numerical investigation of the hydrodynamics of carangiform simming in the transitional and inertial flow regimes," *J. Exp. Biol.* **211**, 1541–1558 (2008).
15. K. H. Low, C. Zhou and Yu Zhong, "Gait planning for steady swimming control of biomimetic fish robots," *Adv. Robot.* **23**, 805–829 (2009).
16. R. Mason and J. W. Burdick, "Experiment in Carangiform Robotic Fish Locomotion," *Proceedings of the 2000 IEEE International Conference on Robotics & Automation*, San Francisco, CA (Apr. 2000).
17. M. Nakashima, N. Ohgishi and K. Ono, "A study on the propulsive mechanism of a double jointed fish robot utilizing self-excitation control," *JSME Int. J.* C **46**(3), 982–990 (2003).
18. C. R. Reeves, J. E. Rowe, *Genetic Algorithms – Principles And Perspectives, A Guide to GA Theory* (Kluwer Academic, Massachusetts, 2003).
19. R. L.Haupt, S. E. Haupt, *Practical Genetic Algorithms*, 2nd ed. (John Willey, San Francisco, CA, 2004).
20. A. W. Moore, *Iterative Improvement Search Hill Climbing, Simulated Annealing, WALKSAT, and Genetic Algorithms* (School of Computer Science Carnegie Mellon University, Pittsburgh, PA, 2009). Available at www.cs.cmu.edu/∼awm
21. M. Hagiwara, "Pseudo Hill Climbing Genetic Algorithm (PHGA) for Function Optimization," *Proceedings of the 1993 International Joint Conference on Neural Networks*, Nagoya Congress Center, Japan (Oct. 25–29, 1993).
22. C. R. Houck, J. A. Joines and M. G. Kay, "A Genetic Algorithm for Function Optimization: A Matlab Implementation," Technical Report NCSU-IE-TR-95-09 (North Carolina State University, Raleigh, NC, 1995).

**Appendix**

$$\begin{bmatrix} M_{11} & M_{12} & M_{13} \\ M_{21} & M_{22} & M_{23} \\ M_{31} & M_{32} & M_{33} \end{bmatrix} \begin{bmatrix} \ddot{\theta}_1 \\ \ddot{\theta}_2 \\ \ddot{\theta}_3 \end{bmatrix} = \begin{bmatrix} N_1 \\ N_2 \\ N_3 \end{bmatrix},$$

where

$$\begin{aligned} M_{11} &= I_1 + m_1 a_1^2 + m_2 l_1^2 + m_3 l_1^2 + m_2 a_2^2 + I_2 + m_3 l_2^2 \\ &\quad + m_3 a_3^2 + I_3 + 2m_2 l_1 a_2 \cos\theta_2 + 2m_3 l_1 l_2 \cos\theta_2 \\ &\quad + 2m_3 l_1 a_3 \cos(\theta_2 + \theta_3) + 2m_3 l_2 a_3 \cos\theta_3 + \pi\rho L C^2 \\ &\quad \cdot \frac{u}{\sqrt{U_m^2 + u^2}} \cdot \sin\alpha \cdot l_1 \cdot (l_1 \cos\theta_1 + l_2 \cos(\theta_1 + \theta_2) \\ &\quad - a_3 \cos(\theta_1 + \theta_2 + \theta_3)) \cdot \{\cos\theta_1 \cdot \cos(\theta_1 + \theta_2 + \theta_3) \\ &\quad + \sin\theta_1 \cdot \sin(\theta_1 + \theta_2 + \theta_3)\}. \end{aligned}$$

$$\begin{aligned} M_{12} &= m_2 a_2^2 + I_2 + m_3 l_2^2 + m_3 a_3^2 + I_3 + m_2 l_1 a_2 \cos\theta_2 \\ &\quad + m_3 l_1 l_2 \cos\theta_2 + m_3 l_1 a_3 \cos(\theta_2 + \theta_3) \\ &\quad + 2m_3 l_2 a_3 \cos\theta_3 + \pi\rho L C^2 \cdot \frac{u}{\sqrt{U_m^2 + u^2}} \cdot \sin\alpha \cdot l_1 \\ &\quad \cdot (l_2 \cos(\theta_1 + \theta_2) - a_3 \cos(\theta_1 + \theta_2 + \theta_3)) \\ &\quad \cdot \{\cos\theta_1 \cdot \cos(\theta_1 + \theta_2 + \theta_3) + \sin\theta_1 \\ &\quad \cdot \sin(\theta_1 + \theta_2 + \theta_3)\}. \end{aligned}$$

$$\begin{aligned} M_{13} &= m_3 a_3^2 + I_3 + m_3 l_1 a_3 \cos(\theta_2 + \theta_3) + m_3 l_2 a_3 \cos\theta_3 \\ &\quad - \pi\rho L C^2 \cdot \frac{u}{\sqrt{U_m^2 + u^2}} \cdot \sin\alpha \cdot l_1 \\ &\quad \cdot (a_3 \cos(\theta_1 + \theta_2 + \theta_3)) \cdot \{\cos\theta_1 \cdot \cos(\theta_1 + \theta_2 + \theta_3) \\ &\quad + \sin\theta_1 \cdot \sin(\theta_1 + \theta_2 + \theta_3)\}. \end{aligned}$$

$$\begin{aligned} M_{21} &= m_2 a_2^2 + I_2 + m_3 l_2^2 + m_3 a_3^2 + I_3 + m_2 l_1 a_2 \cos\theta_2 \\ &\quad + m_3 l_1 l_2 \cos\theta_2 + m_3 l_1 a_3 \cos(\theta_2 + \theta_3) \\ &\quad + 2m_3 l_2 a_3 \cos\theta_3 + \pi\rho L C^2 \cdot \frac{u}{\sqrt{U_m^2 + u^2}} \cdot \sin\alpha \cdot l_2 \\ &\quad \cdot (l_1 \cos\theta_1 + l_2 \cos(\theta_1 + \theta_2) - a_3 \cos(\theta_1 + \theta_2 + \theta_3)) \\ &\quad \cdot \{\cos(\theta_1 + \theta_2) \cdot \cos(\theta_1 + \theta_2 + \theta_3) + \sin(\theta_1 + \theta_2) \\ &\quad \cdot \sin(\theta_1 + \theta_2 + \theta_3)\}. \end{aligned}$$

https://doi.org/10.1017/S0263574711000555 Published online by Cambridge University Press

$$M_{22} = m_2a_2^2 + I_2 + m_3l_2^2 + m_3a_3^2 + I_3 + 2m_3l_2a_3\cos\theta_3 + \pi\rho LC^2 \cdot \frac{u}{\sqrt{U_m^2+u^2}} \cdot \sin\alpha \cdot l_2 \cdot (l_2\cos(\theta_1+\theta_2) - a_3\cos(\theta_1+\theta_2+\theta_3)) \cdot \{\cos(\theta_1+\theta_2) \cdot \cos(\theta_1+\theta_2+\theta_3) + \sin(\theta_1+\theta_2) \cdot \sin(\theta_1+\theta_2+\theta_3)\}.$$

$$M_{23} = m_3a_3^2 + I_3 + m_3l_2a_3\cos\theta_3 - \pi\rho LC^2 \cdot \frac{u}{\sqrt{U_m^2+u^2}} \cdot \sin\alpha \cdot l_2 \cdot (a_3\cos(\theta_1+\theta_2+\theta_3)) \cdot \{\cos(\theta_1+\theta_2) \cdot \cos(\theta_1+\theta_2+\theta_3) + \sin(\theta_1+\theta_2) \cdot \sin(\theta_1+\theta_2+\theta_3)\}.$$

$$M_{31} = m_3a_3^2 + I_3 + m_3l_1a_3\cos(\theta_2+\theta_3) + m_3l_2a_3\cos\theta_3 + \pi\rho LC^2 \cdot \frac{u}{\sqrt{U_m^2+u^2}} \cdot \sin\alpha \cdot a_3 \cdot (l_1\cos\theta_1 + l_2\cos(\theta_1+\theta_2) - a_3\cos(\theta_1+\theta_2+\theta_3)).$$

$$M_{32} = m_3a_3^2 + I_3 + m_3l_2a_3\cos\theta_3 + \pi\rho LC^2 \cdot \frac{u}{\sqrt{U_m^2+u^2}} \cdot \sin\alpha \cdot a_3 \cdot (l_2\cos(\theta_1+\theta_2) - a_3\cos(\theta_1+\theta_2+\theta_3)).$$

$$M_{33} = m_3a_3^2 + I_3 - \pi\rho LC^2 \cdot \frac{u}{\sqrt{U_m^2+u^2}} \cdot \sin\alpha \cdot a_3 \cdot (a_3.\cos(\theta_1+\theta_2+\theta_3)).$$

$$N_1 = 2\pi\rho LC(U_m^2+u^2)\sin\alpha \cdot \cos\alpha \cdot l_1 \cdot \{\cos\theta_1 \cdot \cos(\theta_1+\theta_2+\theta_3) + \sin\theta_1 \cdot \sin(\theta_1+\theta_2+\theta_3)\} - \pi\rho LC^2\dot{\alpha}\sqrt{U_m^2+u^2} \cdot \cos\alpha \cdot l_1 \cdot \{\cos\theta_1 \cdot \cos(\theta_1+\theta_2+\theta_3) + \sin\theta_1 \cdot \sin(\theta_1+\theta_2+\theta_3)\} - \pi\rho LC^2\frac{u}{\sqrt{U_m^2+u^2}} \cdot \sin\alpha \cdot l_1 \cdot \{-l_1 \cdot \dot{\theta}_1^2 \cdot \sin\theta_1 - l_2(\dot{\theta}_1+\dot{\theta}_2)^2 \cdot \cos(\theta_1+\theta_2) + a_3(\dot{\theta}_1+\dot{\theta}_2+\dot{\theta}_3)^2 \cdot \cos(\theta_1+\theta_2+\theta_3)\} \cdot \{\cos\theta_1 \cdot \cos(\theta_1+\theta_2+\theta_3) + \sin\theta_1 \cdot \sin(\theta_1+\theta_2+\theta_3)\} + \dot{\theta}_1 \cdot \dot{\theta}_2 \cdot \{2m_2l_1a_2\sin\theta_2 + 2m_3l_1l_2\sin\theta_2 + 2m_3l_1a_3\sin(\theta_2+\theta_3)\} + \dot{\theta}_1 \cdot \dot{\theta}_3 \cdot \{2m_3l_1a_3\sin(\theta_2+\theta_3) + 2m_3l_2a_3\sin\theta_3\} + \dot{\theta}_2 \cdot \dot{\theta}_3 \cdot \{2m_3l_1a_3\sin(\theta_2+\theta_3) + 2m_3l_2a_3\sin\theta_3\} + \dot{\theta}_2^2 \cdot \{m_2l_1a_2\sin\theta_2 + m_3l_1l_2\sin\theta_2 + m_3l_1a_3\sin(\theta_2+\theta_3)\} + \dot{\theta}_3^2 \cdot \{m_3l_1a_3\sin(\theta_2+\theta_3) + m_3l_2a_3\sin\theta_3\} - (c_1+c_2)\cdot\dot{\theta}_1 + c_2\dot{\theta}_2 - (k_1+k_2)\theta_1 + k_2\theta_2 + T_1.$$

$$N_2 = 2\pi\rho LC(U_m^2+u^2)\sin\alpha \cdot \cos\alpha \cdot l_2 \cdot \{\cos(\theta_1+\theta_2) \cdot \cos(\theta_1+\theta_2+\theta_3) + \sin(\theta_1+\theta_2) \cdot \sin(\theta_1+\theta_2+\theta_3)\} - \pi\rho LC^2\dot{\alpha}\sqrt{U_m^2+u^2} \cdot \cos\alpha \cdot l_2\{\cos(\theta_1+\theta_2) \cdot \cos(\theta_1+\theta_2+\theta_3) + \sin(\theta_1+\theta_2) \cdot \sin(\theta_1+\theta_2+\theta_3)\} - \pi\rho LC^2\frac{u}{\sqrt{U_m^2+u^2}} \cdot \sin\alpha \cdot l_2\{-l_1 \cdot \dot{\theta}_1^2 \cdot \sin\theta_1 - l_2(\dot{\theta}_1+\dot{\theta}_2)^2 \cdot \cos(\theta_1+\theta_2) + a_3(\dot{\theta}_1+\dot{\theta}_2+\dot{\theta}_3)^2 \cdot \cos(\theta_1+\theta_2+\theta_3)\} \cdot \{\cos(\theta_1+\theta_2) \cdot \cos(\theta_1+\theta_2+\theta_3) + \sin(\theta_1+\theta_2) \cdot \sin(\theta_1+\theta_2+\theta_3)\} + \dot{\theta}_1 \cdot \dot{\theta}_3 \cdot \{2m_3l_2a_3\sin\theta_3\} + \dot{\theta}_2 \cdot \dot{\theta}_3 \cdot \{2m_3l_2a_3\sin\theta_3\} - \dot{\theta}_1^2 \cdot \{m_2l_1a_2\sin\theta_2 + m_3l_1l_2\sin\theta_2 + m_3l_1a_3\sin(\theta_2+\theta_3)\} + \dot{\theta}_3^2 \cdot \{m_3l_2a_3\sin\theta_3\} + c_2\dot{\theta}_1 - (c_2+c_3)\dot{\theta}_2 + c_3\dot{\theta}_3 + k_3\theta_1 - (k_2+k_3)\theta_2 + k_3\theta_3 + T_2.$$

$$N_3 = 2\pi\rho LC(U_m^2+u^2)\sin\alpha \cdot \cos\alpha \cdot a_3 - \pi\rho LC^2\dot{\alpha}\sqrt{U_m^2+u^2} \cdot \cos\alpha \cdot a_3 - \pi\rho LC^2\frac{u}{\sqrt{U_m^2+u^2}} \cdot \sin\alpha \cdot a_3 \cdot \{-l_1 \cdot \dot{\theta}_1^2 \cdot \sin\theta_1 - l_2(\dot{\theta}_1+\dot{\theta}_2)^2 \cdot \cos(\theta_1+\theta_2) + a_3(\dot{\theta}_1+\dot{\theta}_2+\dot{\theta}_3)^2 \cdot \cos(\theta_1+\theta_2+\theta_3)\} - \dot{\theta}_1 \cdot \dot{\theta}_2 \cdot \{2m_3l_2a_3\sin\theta_3\} - \dot{\theta}_1^2 \cdot \{m_3l_1a_3\sin(\theta_2+\theta_3) + m_3l_2a_3\sin\theta_3\} + \dot{\theta}_2^2 \cdot \{m_3l_2a_3\sin\theta_3\} + c_3\dot{\theta}_2 - c_3\dot{\theta}_3 + k_3\theta_2 - k_3\theta_3.$$

https://doi.org/10.1017/S0263574711000555 Published online by Cambridge University Press